Microclimatic Buffering by Front-Yard Vegetation: Simulation-Based Assessment of Near-Façade Environmental Modulation in Urban Houses

Indoor Air

WILEY

RESEARCH ARTICLE OPEN ACCESS

Microclimatic Buffering by Front-Yard Vegetation: Simulation-Based Assessment of Near-Façade Environmental Modulation in Urban Houses

Vali Shishebori[1,2] | Nima Izadyar[1,2] | Elmira Jamei[1,2] | Keivan Bamdad[3] | Mahsan Sadeghi[4,5,6]

[1]Built Environment and Engineering Program, College of Sport, Health and Engineering (CoSHE), Victoria University, Melbourne, Australia | [2]Institute for Sustainable Industries and Liveable Cities, Victoria University, Melbourne, Australia | [3]School of Engineering, Design and Built Environment, Western Sydney University, Sydney, Australia | [4]Commonwealth Scientific Industrial Research Organisation (CSIRO), Melbourne, Australia | [5]School of Architecture, Design, and Planning, The University of Sydney, Sydney, Australia | [6]NHMRC Centre for Safe Air, University of Tasmania, Hobart, Australia

Correspondence: Vali Shishebori (vali.shishebori@live.vu.edu.au)

Received: 12 November 2025 | **Revised:** 11 February 2026 | **Accepted:** 17 March 2026

Guest Editor: Poulami Jha

Keywords: buffer zone | ENVI-met simulation | near-façade microclimate | outdoor–indoor interaction | thermal comfort | urban vegetation

ABSTRACT

Residential buildings in low-vegetation urban areas are increasingly exposed to heat and air–pollution stress, particularly in suburbs with limited canopy cover near traffic and industrial sources. This study investigates how front-yard vegetation functions as a near-façade microclimatic buffer, moderating outdoor boundary conditions and providing indicative indoor benefits. High-resolution ENVI-met simulations were conducted for a summer day in inner-western Melbourne, Australia, comparing a fully paved front yard (Base) with a vegetated configuration comprising two deciduous trees and boundary hedges (Green). Microclimatic variables at the outdoor and façade boundary scale, including physiological equivalent temperature (PET), mean radiant temperature (MRT), air temperature (T_a), wind speed and façade temperatures (T_{ow}/T_{iw}) were analysed. Indicative indoor thermal proxies were derived from ENVI-met's simplified indoor module to assess relative differences. At peak hour, vegetation reduced PET and MRT near the façade by 17.1°C and 32.7°C, outside wall temperature (T_{ow}) by 22.0°C, sensible heat flux (H) by 103.1 W/m^2 and shortwave radiation by 283.2 W/m^2. Indoor temperature (T_{in}) proxies showed consistent reductions of 0.1°C–0.2°C, with a cumulative 24-h effect of 1.7°C.h, aligned with façade-scale cooling. Minor changes in T_a and humidity indicate radiative and surface-energy regulation dominate the cooling effect. These results establish front-yard vegetation as a building-scale regulator, modifying façade-level radiative and thermal drivers that influence outdoor–indoor heat and air exchange. The findings establish front-yard greening as a microclimatic strategy under representative hot summer conditions in Melbourne, with broader relevance for low-rise housing in heat-prone, low-vegetation urban areas, motivating future cross-climate studies.

1 | Introduction

Urban areas with limited greenery increasingly face combined heat and air–pollution stress driven by dense built form, traffic emissions and changing climate patterns [1–3]. These outdoor conditions reduce outdoor comfort and intensify indoor heat stress, as urban microclimates and extreme weather events amplify heat transfer through façades and increase infiltration and ventilation loads in buildings [4–6]. Such effects can raise cooling demand by about 25% and keep indoor temperatures (T_{in}) above 26°C for several days, reaching over 29°C during extreme heat events [7]. The combined effect is persistent overheating, degraded indoor air quality (IAQ) and higher energy demand for cooling [8]. Globally, overheating and poor IAQ are now recognised as major public-health and resilience challenges, as people spend most of their time indoors and are exposed to accumulated pollutants and heat [9, 10]. Addressing these challenges requires managing the near-building microclimate to moderate outdoor boundary conditions that govern outdoor–indoor heat and pollutant exchange.

Such management, particularly through vegetation, offers an effective pathway for improving indoor-relevant environmental conditions [11, 12]. Experimental and simulation studies on green walls have demonstrated measurable reductions in façade heat transfer and cooling demand, particularly in humid climates, confirming vegetation's capacity to moderate building envelope thermal loads [13]. Vegetation modifies local environmental drivers through shading, evapotranspiration, particle deposition and changes in airflow, thereby reducing surface heating and decreasing incident radiation before it reaches façades and windows [14, 15]. Extensive research on large-scale urban greening, such as parks, street trees, green roofs and façades, has demonstrated its effectiveness in mitigating urban heat and improving outdoor air quality [16, 17]. However, small-scale private green spaces, including front yards, courtyards and backyards, remain comparatively underexplored, despite their considerable combined area and direct influence at the façade–outdoor interface [18–20]. These private spaces are often excluded from environmental assessment frameworks and design guidance.

Building on these insights, a growing body of research has quantified how vegetation influences outdoor thermal and air quality metrics [21]. Field and measurement studies consistently show that shading and vegetation reduce local air and surface temperatures and improve outdoor comfort conditions [22]. For example, shading from nearby buildings or trees can reduce peak-hour cooling loads by 15%–20%, depending on solar geometry and local context [23]. ENVI-met simulations in typical residential areas demonstrate that denser tree canopies with higher aspect ratios can lower physiological equivalent temperature (PET) by around 3°C and surface temperature by about 3.3°C during summer, confirming the cooling advantage of tree-dominated layouts [24]. Vegetation is also effective at removing or depositing particulate matter and at intercepting some gaseous pollutants, depending on species and canopy structure [25–27]. Yet most prior research continues to treat outdoor microclimate and indoor environmental quality as separate domains: outdoor studies quantify neighbourhood or street-level cooling, whereas building science studies evaluate indoor thermal comfort or IAQ without explicitly linking those outcomes to near-façade microclimatic modification. In Australia, recent synthesis work highlights a lack of systematic indoor monitoring and policy coverage: The *State of Indoor Air in Australia 2025 report* found that very few Australian buildings have been assessed for indoor pollutants and that IAQ standards are absent from building codes [28]. This context underscores the need for clear, transferable evidence that ties outdoor greening to indoor-relevant boundary conditions at the dwelling scale.

Accordingly, four key research gaps remain. First, the near-façade microclimatic buffer zone, where outdoor heat, radiation and airflow are first transformed before entering buildings, has received limited focused investigation, particularly in small residential front yards [29]. Second, few studies simultaneously quantify radiative, convective and façade surface temperature pathways at fine temporal resolution, which are necessary to infer indoor thermal implications [30–32]. Third, there is a lack of locally relevant evidence for low-canopy Australian suburbs, where narrow setbacks and limited public greening amplify the importance of private yard interventions [33]. Fourth, few studies integrate outdoor microclimatic regulation with IAQ processes, often overlooking how vegetation-induced changes in façade temperature, radiation and airflow may influence pollutant infiltration and occupant exposure [34]. Addressing these gaps is vital for advancing the physical understanding of outdoor–indoor thermal and air-quality interactions and for informing design and policy decisions that optimise vegetation placement in residential settings.

In response to these research gaps, this study investigates the role of front-yard vegetation in forming a microclimatic buffer zone around residential buildings in low–vegetation-density urban areas. The primary objective is to quantitatively assess how front-yard vegetation modifies near-façade outdoor microclimatic conditions, including air temperature (T_a), mean radiant temperature (MRT), PET and façade surface temperature, using high-resolution ENVI-met simulations. To support this objective, the study analyses the spatial and temporal variation of these microclimatic effects by comparing a base (nonvegetated) scenario with a vegetated front-yard scenario at multiple near-building and pedestrian-scale locations. By clarifying this analytical focus, the paper contributes to a microclimate-based assessment approach for evaluating small-scale residential greening strategies through façade-level boundary-condition analysis, with relevance to building thermal performance and urban heat mitigation. The paper proceeds as follows: Section 2 outlines the study context, model configuration and simulation design. Section 3 presents the diurnal and spatial microclimate results, highlighting façade-level thermal and radiative dynamics. Section 4 interprets these findings in relation to indoor-relevant mechanisms and implications, and Section 4.3 summarises the main conclusions and identifies directions for future research and practical application.

2 | Methods

This study investigated the effects of private front-yard greenery on near-building microclimate and façade-level boundary conditions relevant to indoor environmental quality in West Melbourne (see Section 2.1), combining urban microclimate modelling with façade-level analysis to evaluate how front-yard vegetation influences outdoor conditions at the building envelope that govern outdoor–indoor environmental interactions. A conceptual buffer-zone approach (Section 2.2) guided by the design of simulation scenarios, variable selection and data interpretation. The ENVI-met model was chosen to capture radiative, convective and aerodynamic processes governing heat and pollutant transport near façades airflow. Indoor environmental conditions were not modelled in detail; instead, indoor relevance is examined through façade-scale microclimatic modification and indicative indoor thermal response derived from ENVI-met outputs.

Microclimatic conditions were simulated using ENVI-met for two scenarios: a paved yard with no vegetation (Base) and a yard with two ash trees and 2-m–high hedges (Green). Three measurement locations captured gradients from the building façade to the pedestrian pathway. Vegetation parameters, including height, crown spread and distance from the façade, were selected according to local council guidelines and buffer zone principles. Meteorological inputs included T_a, relative humidity (RH), wind speed and wind direction. Outputs comprised PET, MRT, T_a, RH, wind speed and direction, as well as outside and inside wall temperature (T_{ow} and T_{iw}) to assess façade thermal response under ENVI-met boundary assumptions. In addition, T_{in} was extracted from ENVI-met's building module and analysed as an indicative proxy of indoor thermal response, enabling comparative assessment between scenarios.

To ensure transparency and reproducibility, the methodological workflow was explicitly segregated into four components: (i) input datasets, including meteorological forcing derived from Bureau of Meteorology (BoM) records, EnergyPlus Weather file (EPW) and urban geometry generated in QGIS; (ii) model configuration, comprising ENVI-met domain setup, boundary conditions, grid resolution and vegetation parameterisation using the Albero library; (iii) output extraction, including time-resolved PET, MRT, T_a, RH, wind fields and façade surface temperatures sampled at predefined locations and heights; and (iv) proxy-based interpretation, in which façade-scale outdoor and indoor outputs were comparatively analysed to quantify relative indoor thermal response and to support mechanism-based discussion of heat transfer across the building envelope and ventilation-related exchange. No field measurements were conducted; all results are based on deterministic ENVI-met outputs under controlled boundary conditions. A graphical workflow summarising the modelling process and analytical steps is provided in Figure 1 to clarify the study structure and sequence of methods used.

2.1 | Study Area

The study site is located in the municipality of Maribyrnong in Melbourne's inner-west, an area characterised by compact building footprints, extensive paved surfaces and limited public greenery. These conditions create pronounced thermal and air quality challenges, making private front yards a critical microclimatic interface between outdoor and indoor environments. The inner-western region of Melbourne, commonly referred to as West Melbourne, typifies a low-canopy urban context where the combined effects of local emissions, climatic extremes and dense morphology contribute to degraded outdoor conditions and potential indoor exposure risks.

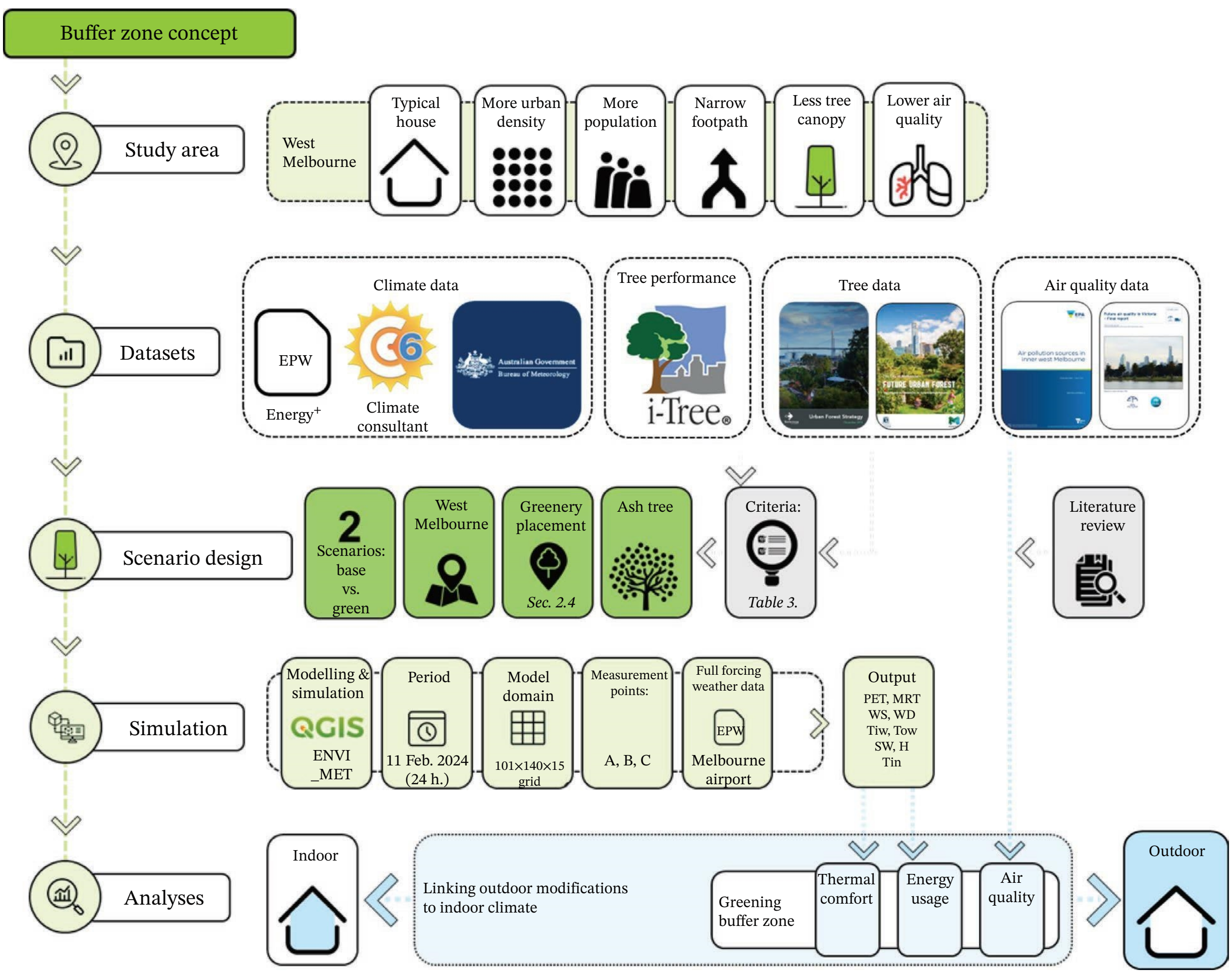

FIGURE 1 | Workflow of the methodology showing the sequence from case study context, datasets, scenario design, model simulation and output analysis.

TABLE 1 | Summary of key environmental indicators for West Melbourne.

Theme	Key data/indicators	Sources
Air pollution sources	• Major contributors: industrial activity, freight corridors, traffic emissions, wood smoke, bushfires and dust storms.	[35]
	• Inner west identified as a hotspot (Brooklyn Industrial Estate exceeds $PM_{2.5}$ limits).	[36, 37]
Pollutant concentrations	• $PM_{2.5}$ often in "fair–poor" range (12.5–50 $\mu g/m^3$), occasionally "very poor" during bushfires. • NO_2 frequently 40–80 ppb near roads; can exceed 80 ppb in hotspots. • O_3 occasionally exceeds 50 ppb. • Local exceedances mainly occur during still, hot summer days or winter wood heating.	[38]
Population and urban growth	• Victoria population projected to reach 11.2 million by 2056 (80% in Melbourne). • Vehicle trips are expected to increase by 10.4 million per day by 2050, worsening urban emissions.	[39]
Temperature patterns	• Mean monthly temperature: ~9°C (July) to > 20°C (January). • Peak summer temperatures > 35°C; winter lows ~0°C. • Many months outside the ASHRAE thermal comfort band.	[40]
Wind patterns	• Northerly and westerly winds dominate in summer and year-round, transporting heat and pollutants. • Afternoon southerlies bring cooling breezes.	[40]
Urban greening	• Tree canopy cover in western suburbs (e.g., Maribyrnong) ≈5.5%, versus higher in eastern suburbs.	[41]
	• State strategy: 30 million trees by 2030.	[42, 43]
	• Narrow setbacks and limited nature strips restrict street tree planting; Relying solely on public land yields max ~10% canopy, below the 20% target.	[44]

Table 1 summarises key environmental indicators derived from official datasets and planning reports, including the 2023 BoM climate records [45], the Melbourne Airport EPW file (analysed using Climate Consultant 6.0 [46]) and state environmental and greening strategies. This table establishes the climatic, pollution and urban-form context that frames the need for microclimate simulations and highlights why front-yard greening is particularly relevant in this region. Air pollution in this region is dominated by industrial activity, freight corridors and traffic emissions, with the inner west consistently identified as a hotspot—particularly around the Brooklyn Industrial Estate, where $PM_{2.5}$ limits are frequently exceeded [35–37]. Typical $PM_{2.5}$ concentrations range from "fair–poor" (12.5–50 $\mu g/m^3$) and can reach "very poor" during bushfires, whereas NO_2 levels near major roads often exceed 80 ppb [38]. Population and traffic projections indicate continued growth in emissions, with Victoria's population expected to reach 11.2 million by 2056 and daily vehicle trips to increase by 10.4 million by 2050 [39].

Climatically, the area experiences strong seasonal variability, with mean monthly temperatures ranging from ~9°C (July) to > 20°C (January), summer peaks above 35°C and winter lows near 0°C [40]. Northerly and westerly winds dominate throughout much of the year, transporting heat and pollutants inland, whereas afternoon southerlies occasionally provide cooling relief. Tree canopy cover across Melbourne's western suburbs—including Maribyrnong—is approximately 5.5%, well below the 20% target of the Victorian Urban Forest Strategy [41–44]. Narrow setbacks, paved surfaces and limited nature strips constrain public greening efforts, reinforcing the role of private yards in achieving local cooling and pollution mitigation.

The selected dwelling represents a typical single-family house type in the suburb, comprising a north-facing front yard, pedestrian pathway, nature strip and backyard. Figure 2 illustrates the site's location and surrounding urban fabric, highlighting its representativeness within the low-canopy, high-density context of Melbourne's inner west. The modelled domain included the target house, two adjacent houses to the east and west and five houses both to the north (street-facing) and south, capturing representative block-scale interactions. The dwelling's north orientation maximises solar exposure while facing the primary street—an active pollution source—providing a relevant case for assessing vegetation as a buffer between traffic emissions and indoor environments. This configuration enables evaluation of how front-yard greening

FIGURE 2 | Study area location in Maribyrnong, West Melbourne, at three spatial scales [47].

modifies microclimatic conditions immediately adjacent to façades, influencing both the quality and temperature of air entering the building under natural ventilation or infiltration conditions.

2.2 | Conceptual Approach: Buffer Zone and Near-Building Climate

The buffer zone refers to the transitional space between the building façade and its property boundary, typically 4–9 m wide in low-rise suburban contexts [41]. It functions as a microclimatic interface where outdoor conditions are modified before interacting with the building envelope. Vegetation within this zone modifies near-building climate through three key mechanisms: (1) shading and radiative attenuation, which reduce incident shortwave radiation and façade surface temperature, (2) evapotranspiration, which cools the surrounding air and enhances local humidity balance; and (3) airflow modulation, which alters infiltration dynamics and pollutant entry rates. Pedestrian-level airflow around buildings is highly sensitive to the built form geometry and near-ground obstructions, and combined wind tunnel and CFD studies show that some configurations can exceed comfort thresholds [13]. These mechanisms govern three primary outdoor–indoor pathways: (i) air quality, by influencing infiltration factors and pollutant penetration rates; (ii) thermal comfort, through reductions in façade temperature and sensible heat transfer. This conceptual approach provides the ENVI-met scenario design in Section 2.5 by linking vegetation design variables, such as canopy structure, distance to façade and barrier height, to measurable indoor-relevant outcomes. Table 2 synthesises representative studies that have demonstrated these linkages for different outdoor interventions, including vegetation, shading devices and façade configurations. A comprehensive version is provided in Appendix Table A1.

As summarised in Table 2, prior studies consistently show that outdoor greening and shading interventions exert measurable effects on both outdoor and indoor environments. Vegetation influences pollutant infiltration by modifying near-surface airflow and deposition processes [48, 49], while also reducing façade surface and T_a through shading and evapotranspiration [51–53]. Tree and hedge configurations positioned closer to façades produce greater reductions in MRT and cooling load, although trade-offs can occur with natural ventilation and pollutant dispersion under certain conditions [22, 50]. Collectively, this highlights the concept of the front yard as a microclimatic buffer zone, providing the empirical justification for the study's simulation focus on vegetation configuration.

Although existing studies provide strong evidence that vegetation and shading can influence both outdoor microclimate and indoor environmental performance, most prior work evaluates these effects either at the scale of open urban spaces or through direct indoor modelling under predefined boundary conditions. The façade-adjacent zone where outdoor microclimatic modifications are first translated into building heat transfer and ventilation-driven exchange remains comparatively underexplored, particularly in the context of small, private residential front yards. Moreover, many studies infer indoor benefits without explicitly framing the near-building microclimate as a distinct physical interface. By conceptualising the front yard as a microclimatic buffer zone, the present study addresses this gap by focusing on façade-level outdoor parameters that govern indoor-relevant processes, thereby providing a mechanism-based bridge between urban vegetation design and indoor environmental implications without directly simulating indoor conditions.

2.3 | Tree Selection

Tree selection followed local council guidelines and urban forest planning reports ensuring both current suitability and long-term resilience under projected climate scenarios. The shortlisting process focused on medium-sized deciduous trees (4–15 m height), which provide sufficient canopy cover without obstructing visibility or exceeding spatial constraints typical of north-facing front yards in low-rise suburban contexts.

Two key sources informed species selection:

1. The Maribyrnong Street Planting Strategy [54, 55], which outlines a 10-year planting program and a list of preferred tree species adapted to local soil, wind and heat conditions; and

TABLE 2 | Key studies linking outdoor intervention to indoor environmental outcomes.

Study/year	Location/ context	Outdoor intervention (type)	Key mechanism(s)	Outdoor effects	Indoor impacts	Outcome category
[48] 2025	South Korea, office	Monitoring + data-driven model	Dynamic ventilation, penetration and removal	Modelled variable penetration and ventilation drivers	Captures indoor $PM_{2.5}$; highlights occupancy and window use effects	IAQ
[49] 2025	Shanghai, residential	Observational	Infiltration and seasonal changes	F_{inf} $PM_{2.5}$ range 0.51–1.16; seasonal variation	Indoor–outdoor $PM_{2.5}$ correlation $R^2 = 0.86$; higher F_{inf} in hot seasons, older buildings, lower floor	IAQ
[25] 2018	CFD case (auditorium)	Trees (varying crown volume coverage)	Deposition, flow modification and ventilation	Indoor concentrations 44%–60% of outdoor under natural ventilation; optimal CVC 2.87–4.73 m^3/m^2	Shows window-opening and tree density effects on indoor PM	IAQ
[22] 2018	Nanjing, China, residential	Grass, shrubs, trees; layouts	Shading, evapotranspiration, layout (Fi index)	MRT ↓ ~6°C–8°C; Ta cooling up to 0.5°C; PM_{10} minor changes	PMV improved (trees: PMV ≈2.6–2.7 vs. 3.3 nongreen); ventilation trade-offs	IAQ and thermal comfort
[50] 2019	Tropical residential	Façade orientation, window operation	Shading and orientation alter solar exposure; window use controls ventilation	Shading ↓ façade exposure; orientation affects solar path	Large unshaded windows: indoor peak 44°C versus 33°C outdoor; shading ↓6.9°C; window opening ↓ T_{in} up to 7.6°C; comfort hours ↑92%	Thermal comfort
[51] 2023	Tempe, AZ (hot-arid)	Building + tree shade	Shade duration and thermal inertia	Continuous shade ↓ LST by 11.3°C; each extra hour shade ≈1°C LST reduction	Shaded façades ~6°C lower surface temps → ↓ heat gains and AC demand	Thermal comfort and energy

(Continues)

TABLE 2 | (CONTINUED)

Study/year	Location/ context	Outdoor intervention (type)	Key mechanism(s)	Outdoor effects	Indoor impacts	Outcome category
[52] 2023	Harbin, China, courtyards	Tree	Shading, wind and evapotranspiration	PET ↓ up to 20.99°C; T_a ↓0.97°C–2.57°C	Cooling energy savings up to ~8%	Thermal comfort and energy
[53] 2018	Multicity	Tree	Shading reduces SW absorbed; evapotranspiration	Exterior wall T ↓ up to 20°C; local air ~1.6°C cooler	Cooling load ↓10%–15.2%; operative temp ↓	Thermal comfort and energy
[23] 2025	Japan, multicity	Trees + buildings	Reduced SW on façade	Peak cooling load ↓15%–20% across cities	Shaded façades at ground floor: strongest load ↓ up to 35% early morning	Energy

2. The City of Melbourne's Future Urban Forest Report [56], which categorises species using a "traffic light" system to show vulnerability under three climate scenarios: current, moderate and extreme.

Species marked as "green" in List A were prioritised, indicating they are currently planted in Melbourne and are not considered vulnerable to projected temperature increases.

Seven species were shortlisted, three species from the *Maribyrnong* strategy and four from the City of Melbourne report. Their environmental performance was assessed using the i-Tree Eco online platform [57], focusing on 20-year projections of carbon sequestration and air pollution removal (CO, O_3, NO_2, SO_2 and $PM_{2.5}$). Input parameters stood for a mature growth stage, in excellent condition, under full sun exposure and found within 0–6 m north of a post-1980 dwelling, consistent with the study context. Energy and stormwater benefits were excluded because i-Tree currently uses U.S. national averages for Australian locations, which are not representative of local conditions or relevant to the present study's microclimatic focus. Reported values are indicative estimates based on USDA Forest Service methodologies, used here to support species comparison rather than absolute quantification.

Table 3 summarises the shortlisted species and their relative environmental performance. This table shows the quantitative diversity among locally suitable tree species in terms of carbon uptake and pollutant removal, providing contextual insight into the broader environmental performance of commonly planted front-yard trees. The velvet ash and chinaberry species, for example, exhibited the highest combined capacity for CO_2 sequestration and particulate removal, aligning with the study's focus on evaluating vegetation's role in façade-level heat and dust mitigation. By quantifying these environmental service differentials, Table 3 supports the contextual framing of vegetation selection within local urban forestry practices. The subsequent ENVI-met simulations focus on a representative deciduous canopy to examine generic vegetation-induced microclimatic buffering effects at the façade scale, rather than species-specific performance.

2.4 | Simulation Tool

A case study model was generated in QGIS Version 3.34, which was used for spatial data preparation, land-use classification and geometric model construction. Microclimatic simulations were conducted using ENVI-met Version 5.7.2, a three-dimensional model widely applied for assessing urban greenery effects on near-building climate, IAQ and thermal comfort [58, 59]. ENVI-met has been extensively validated against field measurements in diverse climatic and urban contexts, providing reliable performance for T_a, MRT and wind speed in near-building environments [60–62]. Accordingly, postprocessing and analysis of simulation outputs were performed using ENVI-met's Leonardo tool, and advanced GIS-based spatial postprocessing was beyond the scope of this study.

Although direct on-site validation was beyond this study's scope, the simulation design followed an evidence-based benchmarking approach that prioritises relative microclimatic contrast over absolute calibration. This approach is widely accepted for scenario-comparison studies [63, 64], where all boundary and material parameters are held constant and only the vegetation configuration varies, ensuring that any systematic model bias affects both scenarios equally and preserves the integrity of differential results. Quantitative benchmarking from prior research consistently reports mean absolute errors below 1°C for T_a, within 5°C for MRT and within 0.5 m/s for wind speed under comparable urban conditions. These error margins fall within recognised thresholds for façade-level and street-canyon analyses, confirming that the model is sufficiently robust to capture the direction, size and spatial distribution of vegetation-induced changes that influence outdoor–indoor environmental interactions.

ENVI-met does not require a formal spin-up period; however, the first two simulation hours were excluded from analysis to allow stabilisation of radiative and soil energy fluxes, consistent with ENVI-met's recommendations. The analysis area was positioned more than 5 H (> 25 m) from lateral boundaries

TABLE 3 | Shortlisted trees and estimated 20-year environmental benefits based on i-Tree calculations.

Source	Tree name (common)	Height (m)	Trunk diameter (m)	Expected benefits ($/20y)	CO_2 equivalent (kg/20y)	Air pollution removal (g/20y)				
						CO	O_3	NO_2	SO_2	$PM_{2.5}$
Maribyrnong Street Planting Strategy [54, 55]	Trident maple	8–12	0.7	406	87	283	13,483	1119	2414	704
	Crepe myrtle	6–10	0.6	85	83	120	5710	474	1022	298
	Bechtel crab apple	6–10	0.6	99	70	219	10,429	865	1867	545
Future Urban Forest Report [56]	Orchid tree	6–10	0.4	334	560	179	8543	709	1529	446
	Mexican hand tree	5–15	0.7	320	170	212	10,094	837	1807	527
	Velvet ash	**5–15**	**0.6**	**425**	**1863**	**319**	**15,181**	**1260**	**2718**	**793**
	Chinaberry tree	8–15	0.45	480	3171	250	11,891	987	2129	621

to minimise edge effects, and cyclic boundary conditions were applied. Ground materials were assigned albedo and emissivity values from the ENVI-met material database, whereas wall and roof properties used default library parameters.

The simulation outputs were configured to be recorded at fixed 1-h intervals. ENVI-met internally uses an adaptive time-stepping scheme at subminute resolution (on the order of seconds) for numerical integration of the fluid dynamics and energy balance equations, responding dynamically to solar height and stability criteria. Only the recorded hourly outputs at 1-h intervals were used for analysis, without additional temporal averaging or median calculation.

The ENVI-met simulations conducted in this study are deterministic, producing a single reproducible output for each scenario under identical boundary and initial conditions. Consequently, the analysis is based on direct scenario-to-scenario comparison of absolute and relative differences, and inferential statistical tests (e.g., t-tests or ANOVA) are not applicable. Observed changes therefore reflect systematic microclimatic responses to vegetation configuration rather than probabilistic variation.

2.5 | Scenario Design

A generic low-rise residential building was modelled with ENVI-met's default wall construction parameters. As the focus of this study is on microclimatic modification rather than material performance, identical wall properties were used for both scenarios to isolate the effects of vegetation on façade energy balance and temperature.

Two scenarios were simulated: (1) Base, standing for a fully paved yard without vegetation, and (2) Green, incorporating two common ash trees (*Fraxinus excelsior*) and 2-m–high hedges along the property boundary. The green scenario included both trees and low-height hedges to be a realistic residential front-yard planting configuration. Trees were the dominant vegetation element in terms of canopy height, shading extent and radiative interception, whereas hedges primarily contributed to the near-ground level. The modelling setup did not aim to isolate the individual effects of trees and hedges; rather, hedges were included as a complementary vegetation layer to reflect typical residential planting practice. This comparative design isolates the influence of vegetation form and placement on the thermal and airflow characteristics of the façade microclimate. The configuration parameters were defined from prior literature and site conditions, as follows:

- The tree–façade distance was set shorter than the building height, following recommended design principles for optimal shading and air exchange [65, 66].
- Hedges were placed along the street boundary (approximately 11 m from the façade) to keep cross-ventilation while intercepting traffic-related pollution and providing privacy.
- Tree height was set to 10 m to balance shading and daylight access while preserving outdoor visibility for visual comfort.
- Consistent with findings from [67], vegetation structure—including canopy density, trunk height and barrier type—was prioritised over greenery coverage alone, as configuration strongly governs microclimatic and pollutant-dispersion outcomes.

This configuration represents a typical, policy-aligned suburban front-yard condition rather than an optimised or parametric design, allowing the analysis to focus on mechanism-based microclimatic responses that are transferable to similar low-rise residential contexts.

Figure 3 shows bird's-eye views of the ENVI-met model for the Base and Green scenarios, illustrating building footprints, vegetation layout and measurement points within the simulation domain. The figure provides a spatial overview of the buffer-zone geometry.

Three measurement locations were defined to assess spatial gradients (Figure 4):

- Location A: near façade, standing for outdoor air immediately adjacent to the façade, relevant for natural ventilation openings and infiltration.
- Location B: midyard, positioned between the two trees to capture microclimatic under direct vegetation influence.
- Location C: at the pedestrian pathway, near the street, serving as the baseline for comparison with shaded and vegetated zones.

Figure 4 shows the corresponding QGIS layout for both scenarios, highlighting the relative placement of vegetation and measurement points. Together, Figures 3 and 4 contextualise the simulation approach by visualising the physical logic of the buffer-zone experiment—a simplified, yet representative, test bed for assessing façade-level mitigation mechanisms.

Vegetation was parameterised using generic tree and hedge objects from ENVI-met's default Albero library. The selected common ash (*F. excelsior*) model includes predefined canopy geometry and vertical leaf area density (LAD) profiles derived from the Albero database. Explicit species-specific physiological parameters, such as customised leaf area index (LAI), LAD or stomatal conductance, were therefore not recalculated, and default library values (e.g., LAD = 1) were applied. Although this approach does not capture detailed interspecies variability, it provides a standardised and internally consistent

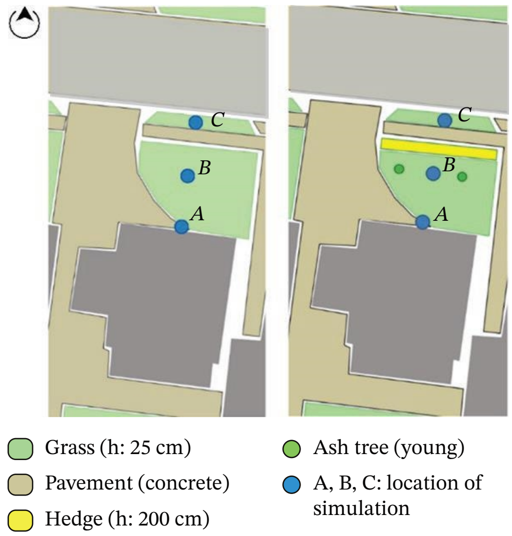

FIGURE 4 | QGIS model setup, Base (left) versus Green (right) scenarios, location (A) near façade, (B) mid-yard and between trees and (C) pedestrian path.

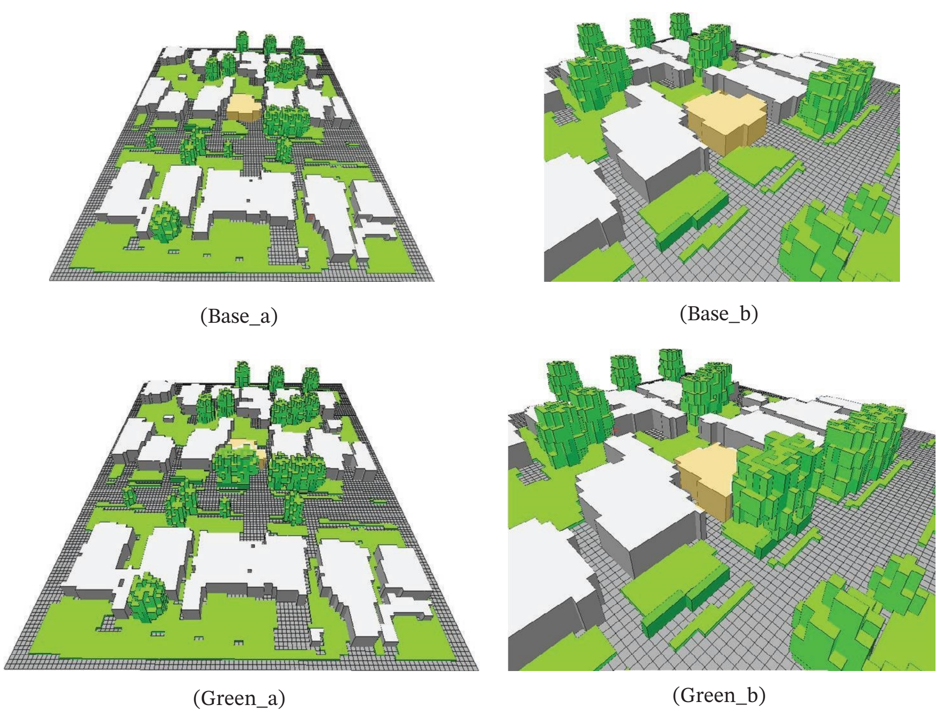

FIGURE 3 | Bird's-eye view of the ENVI-met model (looking from north to south) for Base and Green scenarios, showing building footprints, vegetation layout, measurement points (a–c) and surrounding urban context.

TABLE 4 | Summary of simulation setup and output indicators.

Category	Details	Notes/parameters
Location	West Melbourne, Australia	See Section 2 for urban and climatic context
Simulation tool	QGIS v3.34	Generation of urban layers and model domain
	ENVI-met v5.7.2	3D microclimate model for urban–vegetation–building interactions
Model domain	Front yard and surrounding urban context	Includes two houses to the west (35 m), two to the east (35 m), five to the north including street (50 m) and five to the south (50 m) to represent the block context, grid resolution: 1 × 1 × 2.5 m (first 2.5 m grid split to five grids in Z axis), grid dimensions: 101 × 140 × 15 grids
Building model	Generic low-rise residential	5 m height
Scenarios	Base: No vegetation	Vegetation layout follows local council planting guidelines
	Green: Two ash trees +2 m hedges	SimID: OVrjJAcsGN (base), WM7ORgRlGO (green)
Simulation settings	Period	24 h, summer day, 11 February, 6:00 AM–12 February, 6:00 AM
	Building material	Default wall, moderate insulation, ENVI-met ID: 000000, width = 0.31 m
	Land surface material	Asphalt road, ENVI-met ID: 0200ST, albedo 0.12, emissivity 0.90, z0 roughness length 0.01 m; Pavement concrete (used/dirty), ENVI-met ID: 0200PP, albedo 0.25, emissivity 0.90, z0 roughness length 0.01 m
Measurement points	Three locations	(A) Adjacent to façade, X = 65, Y = 52; (B) midyard, X = 61, Y = 53 and (C) pedestrian path, X = 56, Y = 54—used to assess spatial gradients
	Height	1.75 m (representative pedestrian level)
Vegetation parameters	Trees	Common ash (young), ENVI-met ID: 010080, seasonal leaf factor = 1.0, height = 10.15 m, width = 6.51 × 6.52 m, tree–façade distance = 5.40 m, tree–street distance = 5.40 m, tree–tree distance = 6.00 m (defined according to buffer zone design principles)
	Hedges	Hedge dense, ENVI-met ID: 0200H2, height: 2 m, length: 10.60 m
	Grass	Grass 0.25 m, ENVI-met ID: 0200XX
Boundary conditions	Meteorological full forcing	T_a, RH, wind speed and direction and solar radiation from EPW file (Melbourne airport)

(Continues)

TABLE 4 | (CONTINUED)

Category	Details	Notes/parameters
Output indicators	Microclimate	PET, MRT, T_a, RH, WS and WD
	Façade	Outside and inside wall temperature
	Indoor (indicative)	T_{in} (used as indicative thermal proxy), set to 20.0 °C for the start of simulation
Human energy balance (PET)	Default ENVI-met settings	35-year-old male, 1.75 m, 75 kg, standing posture; surface area = 1.91 m^2; summer clothing = 0.50 clo; metabolic rate = 164.5 W; preferred speed = 1.34 m/s

representation of canopy shading and evapotranspiration processes. This parameterisation is appropriate for the present comparative, scenario-based analysis, which focuses on relative near-façade microclimatic responses between Base and Green configurations rather than absolute species-level biophysical performance.

The simulations represent a typical clear summer day (11–12 February) with no mechanical ventilation. T_{in} was extracted using ENVI-met's building module and analysed as an indicative proxy of indoor thermal response. This indoor representation follows a simplified, lumped thermal formulation and does not explicitly model building services, occupancy, ventilation control or internal heat gains. Pollutant transport ($PM_{2.5}$ and NO_2) was not explicitly simulated; therefore, IAQ implications are inferred from façade-scale microclimatic regulation (radiation, façade surface temperature and near-façade airflow) and their potential influence on indoor boundary conditions. All surfaces, boundary conditions and meteorological inputs were kept identical between scenarios to isolate vegetation effects.

Table 4 summarises the simulation domain, boundary conditions, vegetation characteristics and output indicators used in the ENVI-met modelling, providing a clear reference for scenario design and later analyses.

2.6 | Indicative Indoor Thermal Proxy Modelling

To provide a quantitative linkage between façade-scale microclimatic modifications and indoor-relevant conditions, an indicative indoor T_a proxy was derived using the ENVI-met building module. This module represents the building interior as a simplified single thermal zone dynamically coupled to the surrounding outdoor microclimate, enabling estimation of indoor T_a responses to changes in façade surface temperature, near-façade air conditions and surface heat fluxes.

In the present study, indoor T_a outputs were extracted for both the Base and Green scenarios over the full simulation period. The indoor environment was treated consistently across scenarios, with identical building geometry, material properties and boundary conditions, such that differences in indoor T_a arise solely from vegetation-induced changes in outdoor microclimatic forcing at the building envelope.

The resulting T_{in} is used here as a comparative indicator rather than as a full indoor thermal comfort assessment. No indoor comfort indices, HVAC system behaviour or occupant interactions were modelled. Instead, T_{in} serves as an indicative proxy to evaluate the relative direction and magnitude of indoor thermal response associated with façade-scale cooling effects.

2.7 | Simulation Assumptions and Quality Control

First two simulation hours were excluded to allow stabilisation of radiative and soil energy fluxes, consistent with ENVI-met guidance. No formal sensitivity analysis was performed, as the study is aimed at isolating the relative contrasts between the Base and Green scenarios under identical boundary conditions. To manage potential uncertainty arising from vegetation density, leaf-area parameters and wind direction, hourly outputs at 1-h intervals of key indicators were reported rather than single-time outputs, reducing transient variability. All boundary conditions, material properties and meteorological inputs were held constant to preserve internal comparability, ensuring that any systematic model bias affected both scenarios equally. Model consistency was checked through inspection of energy-balance closure, radiative fluxes and physically realistic diurnal temperature trends, providing confidence in the robustness of the simulation outputs.

Although ENVI-met resolves near-façade airflow, thermal stratification, and radiative exchanges, the present simulations were conducted in microclimate mode and did not activate pollutant routines. No pollutant emissions, dispersion, chemical transformation, dry deposition or outdoor-to-indoor contaminant transport were modelled ($PM_{2.5}$, PM_{10}, and NO_2). IAQ implications are inferred qualitatively from vegetation-induced changes in microclimatic drivers such as airflow patterns, thermal gradients and radiative exposure that influence infiltration and deposition pathways, and are reported as directional, mechanism-based implications rather than quantified indoor pollutant outcomes. The results, therefore, indicate the direction, magnitude and spatial localisation of potential IAQ-relevant effects at the building envelope and should be interpreted as boundary-condition evidence to inform subsequent coupled indoor IAQ or CFD-based pollutant transport modelling (e.g., using CONTAM and CFD solvers such as OpenFOAM or COMSOL).

3 | Results

This section presents the simulated 24-h summer microclimatic and façade responses for the Base and Green scenarios. Hourly outputs were generated at 1-h intervals from the model output files. These hourly values are the recorded state of microclimatic variables after internal simulation calculations. The first two simulation hours were excluded from all analyses to avoid spin-up artefacts and ensure radiative, surface and soil energy fluxes, as well as associated near-surface microclimatic fields, had reached a quasi-steady state. Results are analysed at three locations representing spatial gradients from the building façade (A) to the mid-yard (B) and the pedestrian pathway (C). The analysis focuses on key outdoor indicators—PET, MRT, T_a, RH, wind and wall surface temperature—to assess how vegetation moderates near-building conditions that influence indoor comfort and air quality.

3.1 | PET

Figure 5 presents the diurnal variation in PET across the three measurement locations: the façade (A), mid-yard (B) and pedestrian pathway (C). These graphs illustrate how vegetation influences outdoor thermal conditions immediately next to the building, providing the basis for assessing potential effects on indoor comfort and air quality.

Under the Base scenario, PET values peaked between 12:00 and 16:00, exceeding 50°C near the façade (Location A) and indicating extreme thermal stress conditions. In contrast, the Green scenario, which includes two ash trees and hedges, substantially reduced daytime PET at Locations A and B. The greatest improvement occurred near the façade, where peak PET decreased by 17.1°C at 15:00 compared with the Base case. This reduction represents a shift from conditions classified as strong to extreme heat stress toward moderate heat stress levels, indicating a substantial improvement in outdoor thermal exposure during peak afternoon hours. At the mid-yard position, the reduction of 12.4°C at 16:00, whereas the pedestrian pathway (Location C) showed only a marginal change (0.7°C at 17:00), confirming that the effect of vegetation was concentrated within the immediate buffer zone.

Considering the Base scenario alone, Location A is 5.4°C warmer than Location C at 15:00, demonstrating that near-building conditions were significantly less comfortable in the absence of greenery. This highlights the amplifying role of façades in heat accumulation through reflected and re-radiated solar energy, reinforcing the need for façade-adjacent greening. Night-time PET values were nearly identical in both scenarios, suggesting that the influence of vegetation was primarily diurnal and dominated by shading and evapotranspiration rather than by residual thermal storage. Figure 5b summarises the distribution of hourly PET values over the 24-h period for all locations using box-and-whisker plots, where the box represents the interquartile range, the central line denotes the median, and the cross marks the mean; the results show mean PET reductions of 4.7°C at Location A and 3.4°C at Location B, with negligible change at Location C. These results highlight the strong localised cooling effect of front-yard vegetation and confirm that vegetation most effectively improves microclimatic comfort close to façades.

The pronounced PET reductions in the Green scenario underscore the combined influence of shading and evapotranspiration in lowering radiant and convective heat loads at pedestrian level. Tree canopies intercept direct solar radiation, while evapotranspiration enhances latent cooling, thereby improving local thermal sensation. The observed reduction in PET peaks also indicates the buffering capacity of vegetated surfaces, which absorb direct solar radiation.

3.2 | MRT

Figure 6 illustrates the diurnal variation in MRT across the three measurement locations: the façade (A), mid-yard (B) and pedestrian pathway (C). These results capture the radiative component of the microclimate, indicating how surface shading and vegetation modify exposure to solar and longwave radiation near buildings.

Under Base conditions, MRT peaked between 11:00 and 16:00, exceeding 66°C near the façade (Location A) and highlighting the intense radiative load imposed by direct and reflected sunlight. In the Green scenario, MRT values were markedly reduced at Locations A and B, with the largest decrease observed near the façade, where peak MRT was lowered by 32.7°C at 15:00 compared with the Base case. Beneath the tree canopy, MRT remained about 26.0°C lower than the Base scenarios at 16:00, compared with Location C with minor changes (maximum reduction of 1.1°C at 17:00 and 18:00), reflecting the combined shading and evapotranspiration effects of vegetation. Night-time MRT values were comparable across scenarios, indicating limited nocturnal influence.

In the Base scenario, Location A was 5.1°C warmer than Location C at 15:00, confirming the façade's role in amplifying radiant heat stress under unshaded conditions. Minimum, mean and maximum MRT values for 24 h (Figure 6b) further illustrate these cooling effects, showing absolute mean differences of 9°C at Location A and 7.1°C at Location B, with negligible change at Location C. These results demonstrate the critical role of vegetation in reducing radiative heat loads at the façade–yard interface, reinforcing the effectiveness of near-building greening as a passive cooling strategy.

3.3 | T_a

Figure 7 shows the diurnal change in T_a across the three measurement locations: the façade (A), mid-yard (B) and pedestrian pathway (C). Unlike PET and MRT, diurnal T_a patterns show minimal differences between the Base and Green scenarios, indicating that vegetation had a relatively limited influence on the overall T_a within the small front-yard domain.

The maximum temperature differences were 0.9°C at Location A at 15:00 and 0.7°C at Location B at 16:00 under the Green scenario. Minimum, mean and maximum Ta values for 24 h (Figure 7b) further confirm these minor variations, showing

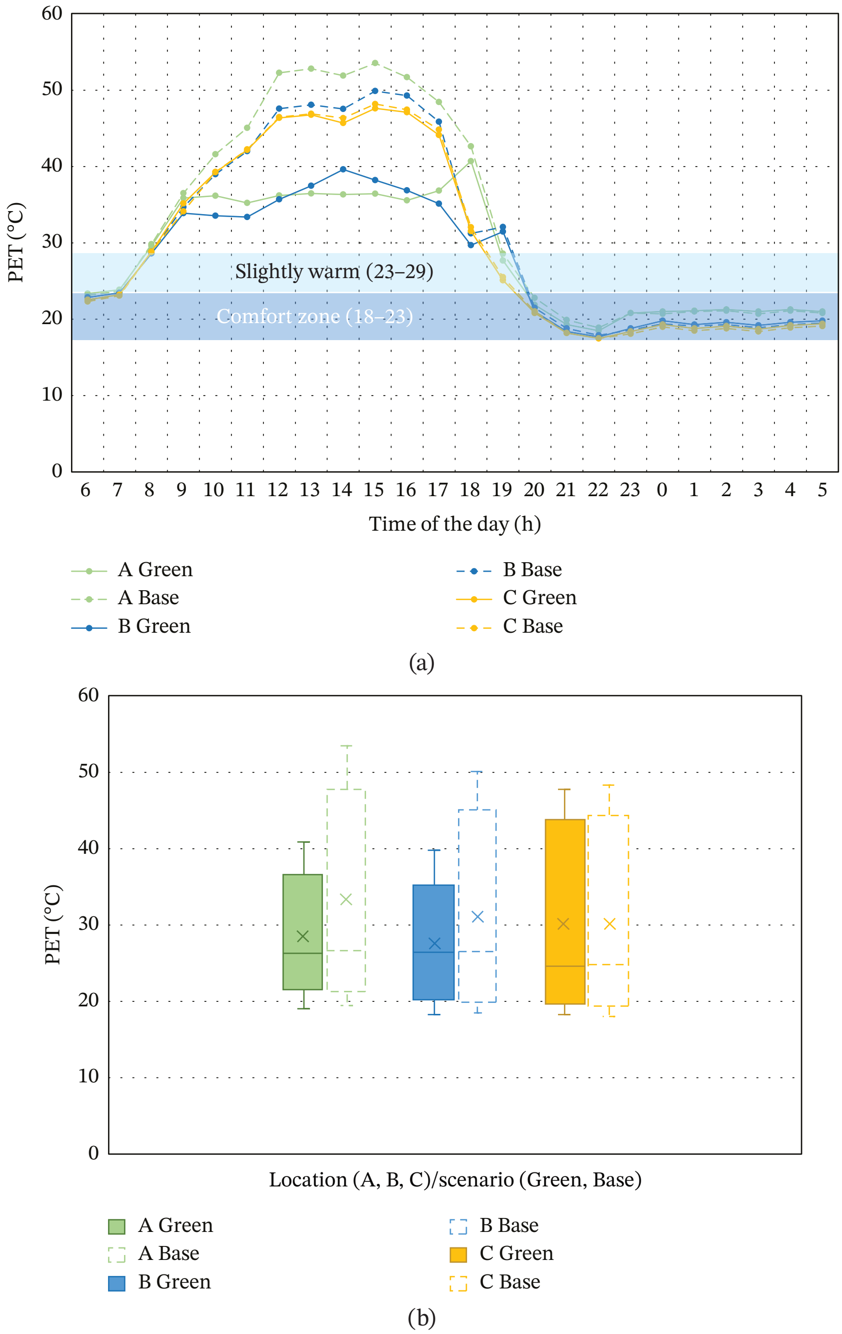

FIGURE 5 | Comparison of PET at three locations for both scenarios based on (a) diurnal trend; (b) distribution of hourly values, showing minimum, maximum, median (line) and mean (×).

mean reductions of 0.2°C at Location A and 0.1°C at Location B, with no noticeable change at Location C. The limited T_a response compared with the substantial reductions observed in PET and MRT reflects the highly localised nature of T_a modification and the dominant role of radiative rather than convective processes in near-building thermal regulation.

These findings indicate that while vegetation can meaningfully moderate radiant and surface heat loads, its impact on bulk T_a is minor within small residential yards. Nevertheless, even small T_a reductions may contribute to improved perceived comfort when combined with the significant PET and MRT cooling effects reported earlier.

3.4 | RH

Patterns of RH are presented in Figure 8 for the three monitored locations: façade (A), mid-yard (B) and pathway (C). The overall diurnal trend shows a typical inverse relationship with T_a, with RH lowest in the early afternoon and highest overnight. Differences between the Base and Green scenarios were modest but consistent, with slightly elevated RH levels under vegetated conditions during the warmest hours of the day.

Between 14:00 and 17:00, RH in the Green scenario rose by 1.9%–2.5% at Location A and 1.9% at Location B at 16:00 and 17:00 compared with the Base case. These small increases are

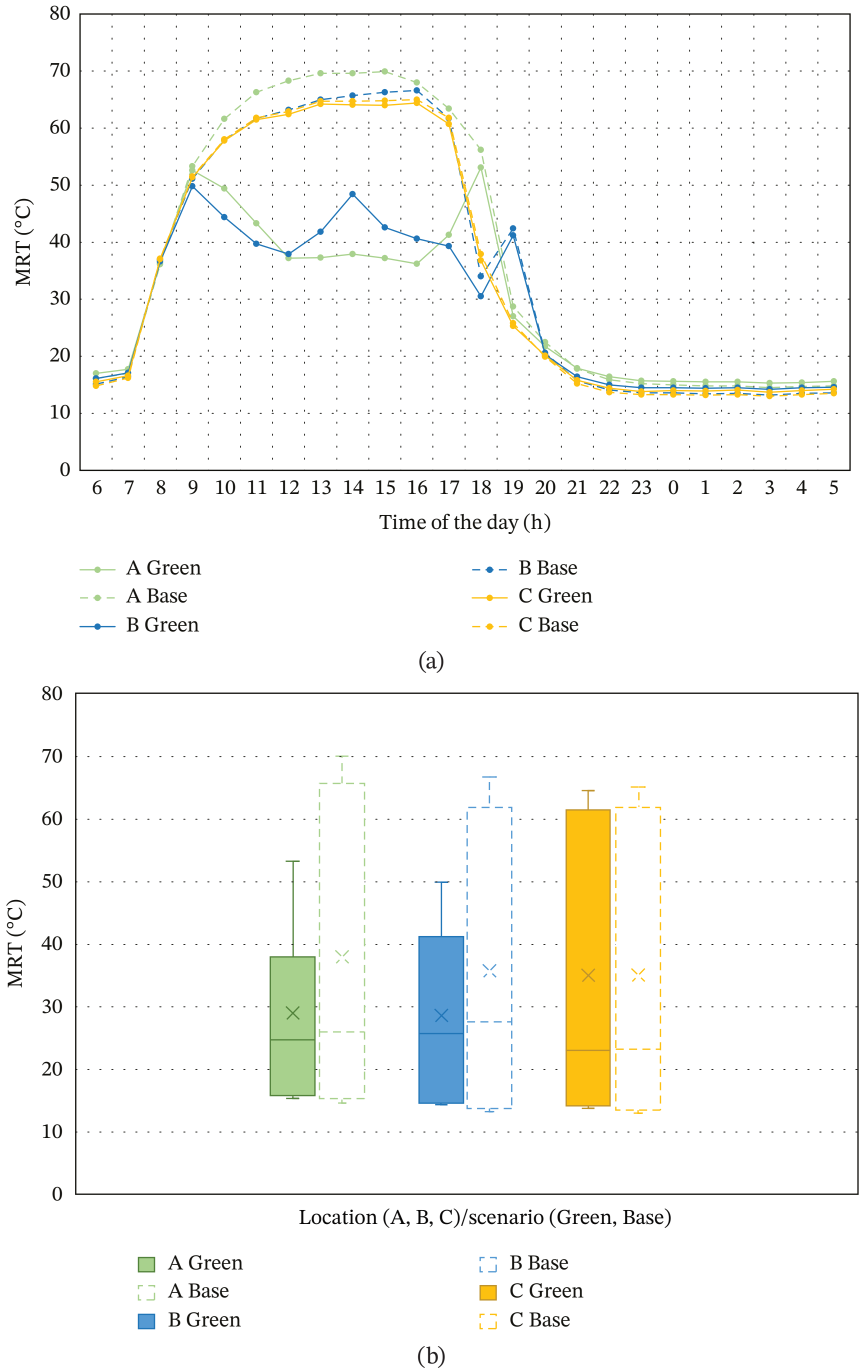

FIGURE 6 | Comparison of MRT at three locations for both scenarios based on (a) diurnal trend; (b) distribution of hourly values, showing minimum, maximum, median (line) and mean (×).

attributed to evapotranspiration from trees and hedges, which released moisture into the near-surface air and marginally reduced drying potential. Minimum, mean and maximum values for 24 h (Figure 8b) indicate mean increases of 0.7% at Location A, 0.5% at Location B and 0.2% at Location C, confirming that vegetation primarily affected local humidity close to the façade.

Although the magnitude of RH change is limited, this response is physically expected for small-scale residential vegetation. At the front-yard scale, evapotranspiration contributes secondary latent cooling, whereas reductions in radiant load and surface temperature dominate thermal comfort improvements. Consequently, the modest RH increase complements the substantial reductions observed in PET and MRT without introducing humidity-related discomfort, reinforcing the role of vegetation as a microclimatic buffer rather than a moisture-dominant modifier.

3.5 | Wind Speed and Wind Direction

Figure 9 depicts the diurnal variation in wind speed and direction across the three monitored locations. Overall, wind patterns remained stable between the Base and Green scenarios,

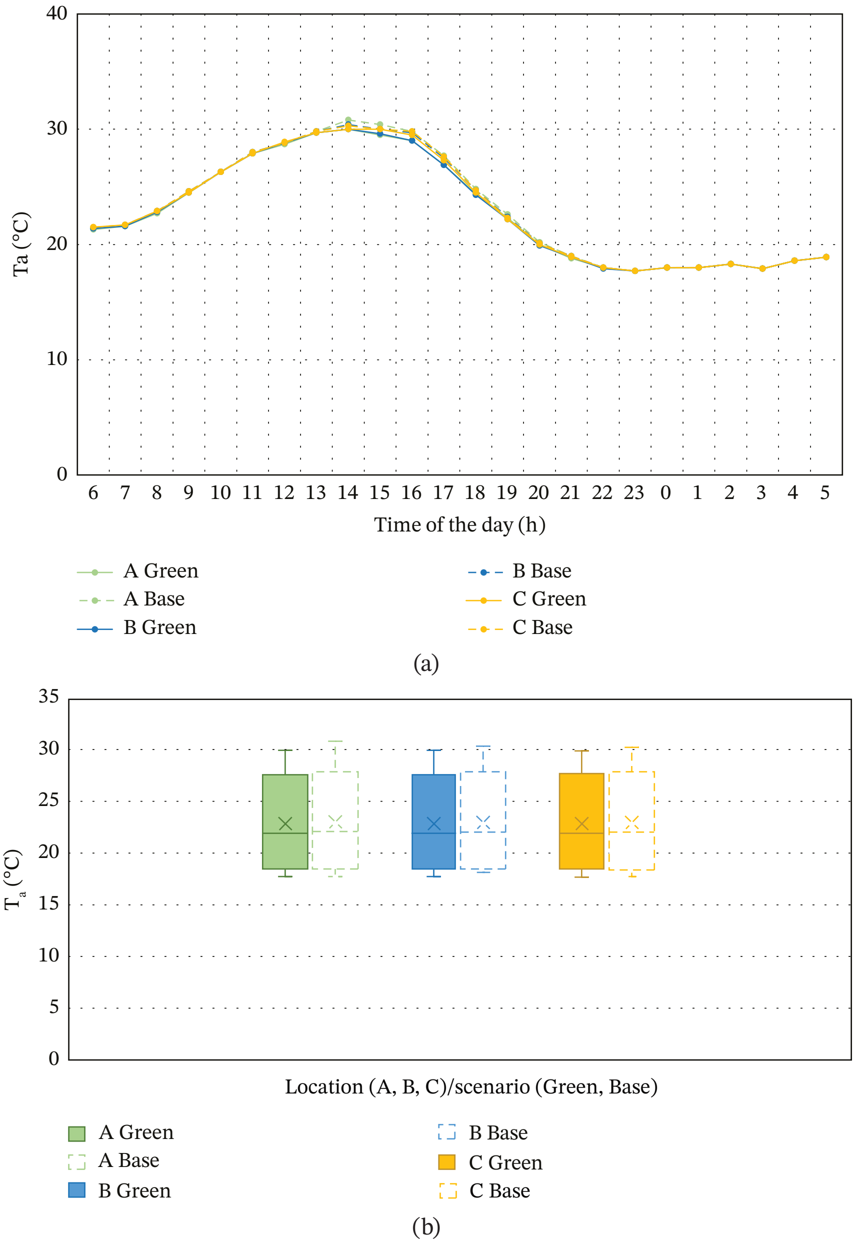

FIGURE 7 | Comparison of T_a at three locations for both scenarios based on (a) diurnal trend; (b) distribution of hourly values, showing minimum, maximum, median (line) and mean (×).

suggesting that the introduced vegetation exerted only minimal aerodynamic influence on airflow within the small front-yard domain.

At all locations, two modest wind speed peaks occurred around midmorning and late evening, consistent with the prevailing east-to-west flow. Mean daytime wind speeds were slightly higher under the Green scenario, with marginal increases of about 0.1 m/s at Locations A and B, and no discernible difference at Location C (Figure 9d). These small variations likely reflect subtle deflection and channelling effects produced by tree trunks and hedges rather than large-scale turbulence alteration.

Wind direction patterns were virtually unchanged, maintaining a dominant east-to-west trajectory throughout both scenarios. The persistence of these flow characteristics indicates that local vegetation influenced near-surface mixing without modifying the broader wind regime—a useful finding for understanding ventilation behaviour and pollutant dispersion near building façades.

3.6 | T_{ow}/T_{iw}

Figure 10 compares the diurnal variation of T_{ow} and T_{iw} under Base and Green scenarios. The façade surface showed a pronounced cooling response to vegetation shading. Under Base conditions, the T_{ow} climbed sharply after 10:00 h, peaking at 54.0°C around 14:00 h. With vegetation, the corresponding peak was delayed to 16:00 h and limited to 42.5°C, representing

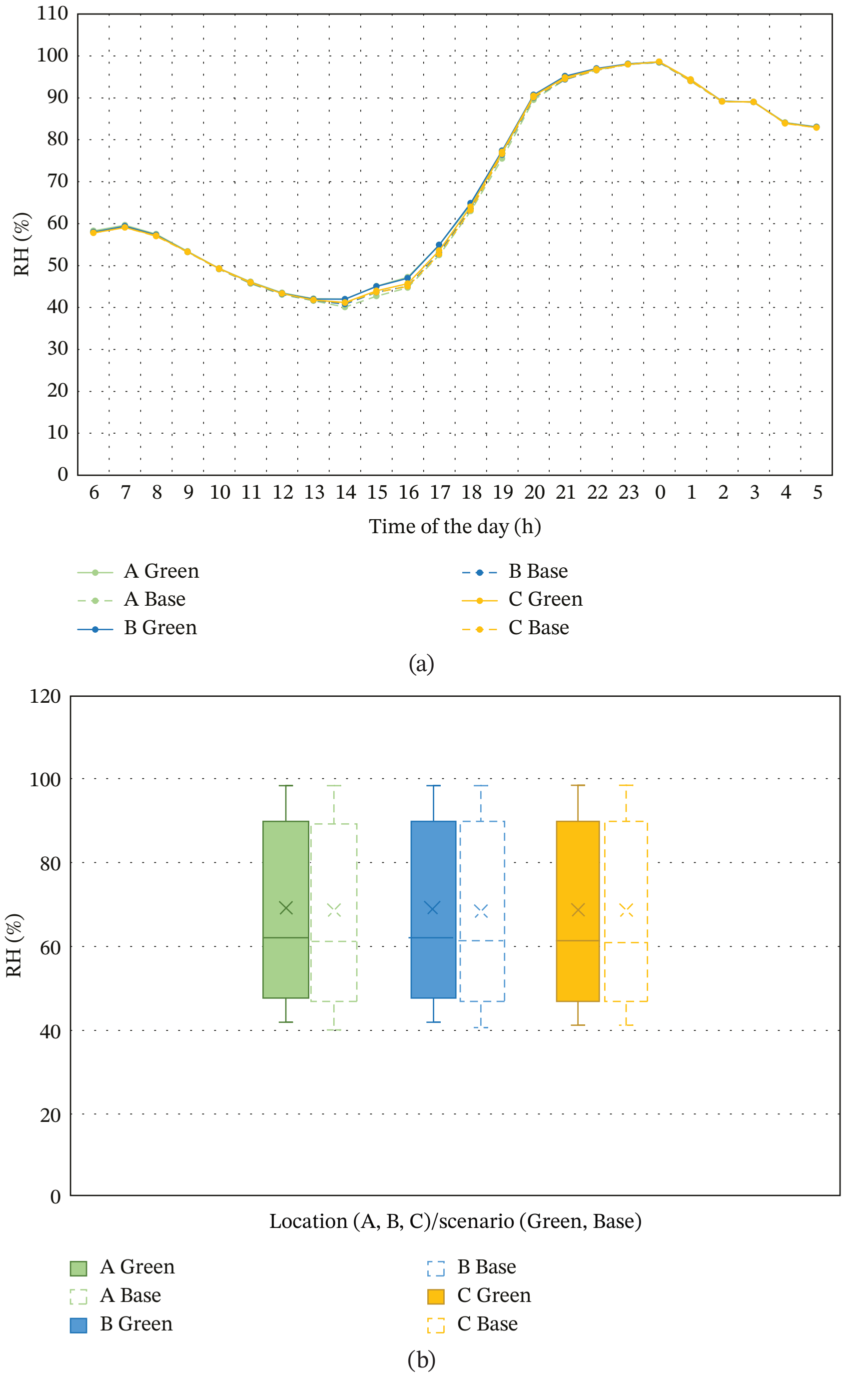

FIGURE 8 | Comparison of RH at three locations for both scenarios based on (a) diurnal trend; (b) distribution of hourly values, showing minimum, maximum, median (line) and mean (×).

a 22°C reduction in maximum surface temperature at 14:00 (Figure 10a). The diurnal summary for 24 h (Figure 10b) indicates an average decrease of 4.4°C, whereas the façade's temperature amplitude contracted from 36.5°C (Base) to 24.9°C (Green)—an 11.7°C reduction in daily fluctuation, demonstrating improved thermal stability at the building envelope.

T_{iw} followed the same trend but with smaller amplitude. Beginning near 20°C, internal wall temperatures rose slightly throughout the day, reaching 23.1°C in the Base case and 22.4°C in the Green scenario (Figure 10a). This corresponds to a 0.7°C peak difference and an average reduction of 0.4°C (Figure 10b).

Complementing the time-series analysis, Figure 11 provides a spatial comparison of façade surface temperature distributions at 3-h intervals, highlighting the progressive effects of vegetation shading across the day. In the early morning (06:00–09:00), both scenarios show uniformly cool façades below 23°C. By midday (12:00–15:00), distinct thermal divergence becomes clear. Under the Base scenario, the façade absorbs substantial solar radiation, with substantial portions exceeding 50°C at 15:00 (Figure 11), particularly on the central and lower panels directly exposed to sunlight. In contrast, the Green scenario exhibits a noticeably cooler and more heterogeneous surface pattern, where shaded zones remain below 35°C and unshaded regions range between 38°C and 47°C.

As can be seen from Figure 11, during the late afternoon (18:00), the Base façade keeps residual heat, whereas the Green façade cools more rapidly due to lower radiative storage and convective release enhanced by vegetation. By evening and overnight (21:00–03:00), both façades return to near-uniform temperatures below 25°C. The temporal and spatial patterns collectively confirm that vegetation not only reduces daytime peak façade temperatures but also mitigates lateral heat concentration, yielding a more stable and thermally balanced façade surface throughout the diurnal cycle.

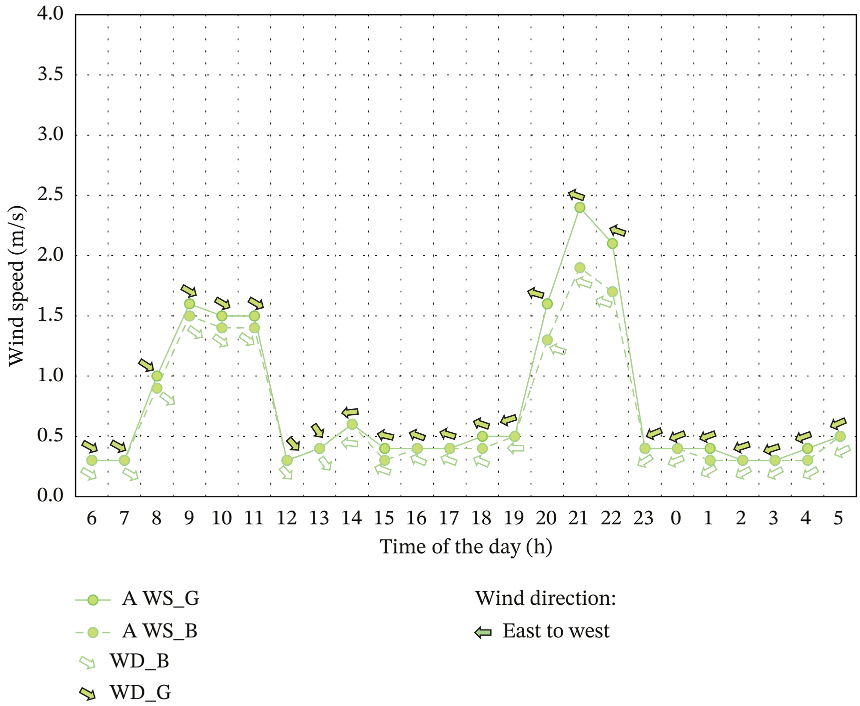

(a)

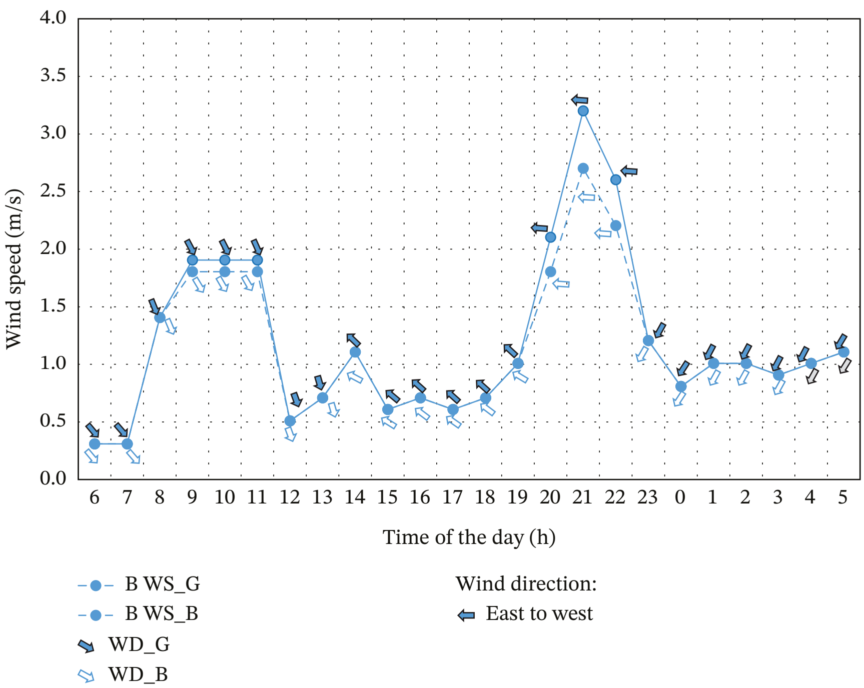

(b)

FIGURE 9 | Diurnal WS for both scenarios at (a) Location A; (b) Location B; (c) Location C; (d) distribution of hourly values, showing minimum, maximum, median (line) and mean (×) across all locations.

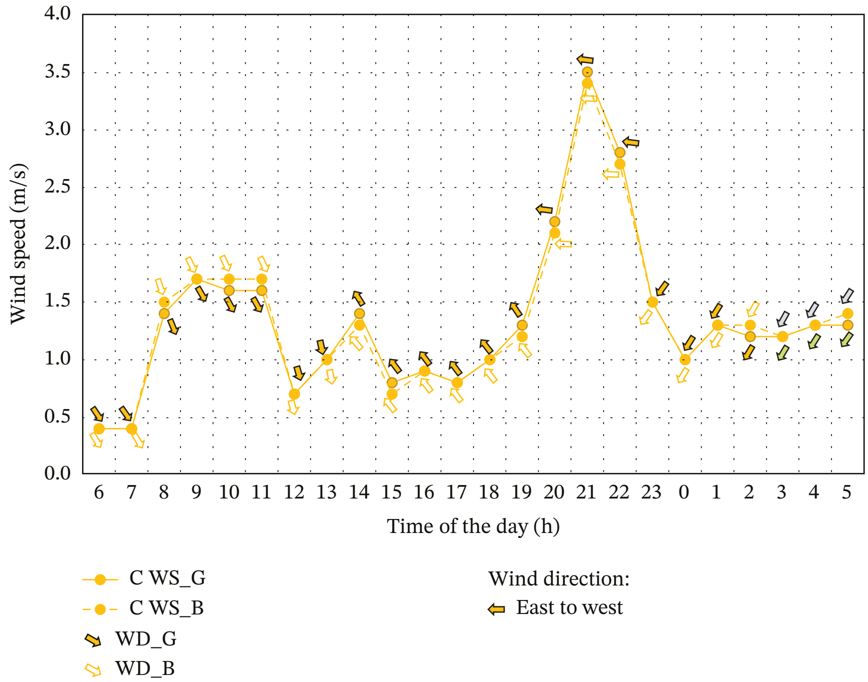

(c)

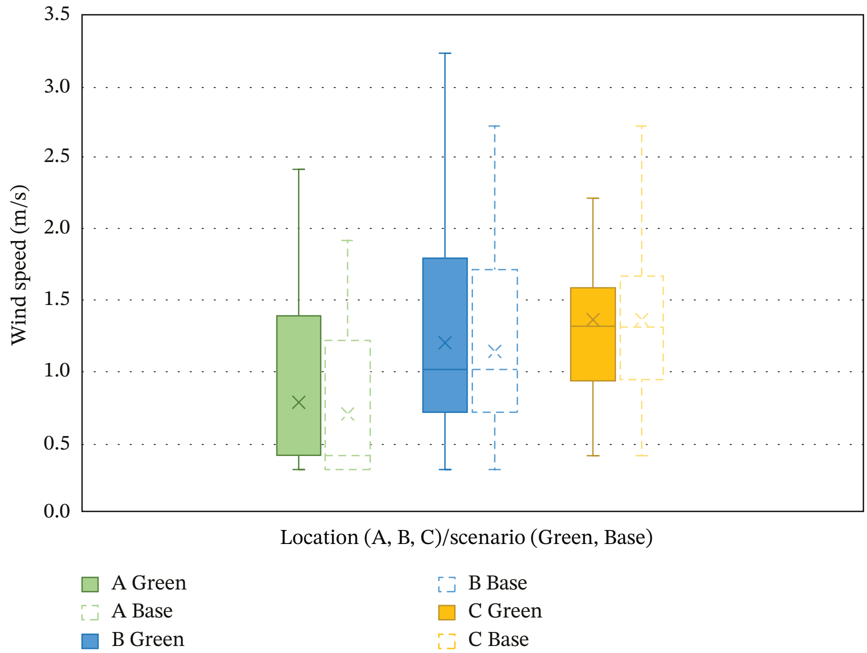

(d)

FIGURE 9 | **(CONTINUED)**

3.7 | Shortwave Radiation and Sensible Heat Flux (H)

Figure 12 presents the diurnal variation of shortwave radiation (received and absorbed) and H for both scenarios. Under the Base condition, shortwave radiation received (SW_{rec}) rose rapidly from morning and peaked at 13:00, reaching 555.4 W/m^2, whereas shortwave radiation absorbed (SW_{abs}) peaked at 333.3 W/m^2 at this time. In the Green scenario, vegetation shading led to substantial reductions at 13:00, with SW_{rec} and SW_{abs} reduced to 83.4 and 50.1 W/m^2, respectively. The maximum SW_{rec} in the Green scenario occurred later in the afternoon (16:00), reaching 364.4 W/m^2, which is 191.1 W/m^2 lower than the Base peak (approximately 34% reduction).

H exhibited a similar temporal pattern. Under Base conditions, H peaked at 15:00, reaching 130.0 W/m^2. In contrast, the Green scenario showed a value of 41.4 W/m^2 at the same time, with its peak occurring later (17:00) at 79.6 W/m^2 (50.4 W/m^2 lower than the Base peak) (~39% reduction). The delayed and

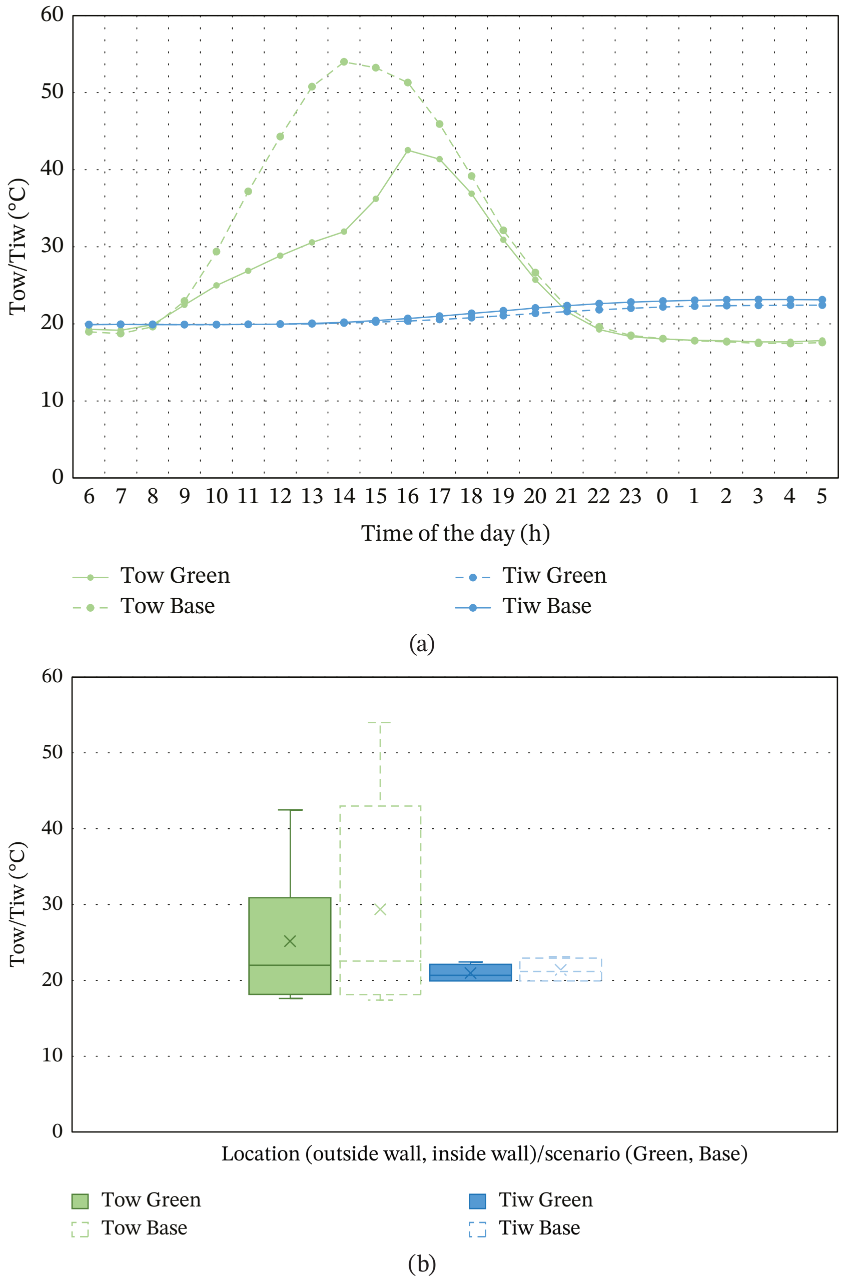

FIGURE 10 | Comparison of outside/Inside wall temperature for both scenarios based on (a) diurnal trend; (b) distribution of hourly values, showing minimum, maximum, median (line) and mean (×).

dampened peaks of both SW_{rec} and H under the Green scenario confirm the strong role of vegetation in attenuating direct solar gains and moderating convective heat transfer at the façade surface.

3.8 | Indicative T_{in}

Figure 13 presents the simulated indoor T_a profiles for the Base and Green scenarios over the 24-h period. T_{in} followed a similar diurnal pattern in both cases, with slightly lower values consistently observed under the Green scenario. The maximum indoor T_a reached 22.9°C in the Base scenario and 22.8°C in the Green scenario, whereas mean T_{in} differed by 0.1°C. Peak-hour differences were on the order of 0.1°C–0.2°C, indicating a modest but systematic indoor response associated with façade-scale microclimatic modification.

The largest differences occurred during the late evening to early night (22:00–02:00), which aligns with the peak divergence in interior wall temperature (T_{iw}), reflecting the role of envelope thermal inertia in mediating indoor conditions. Over the full 24-h simulation, the cumulative indoor cooling effect amounted to 1.7°C.h, demonstrating that the Green façade scenario produces a persistent, albeit small, relative T_{in} reduction (Table 5).

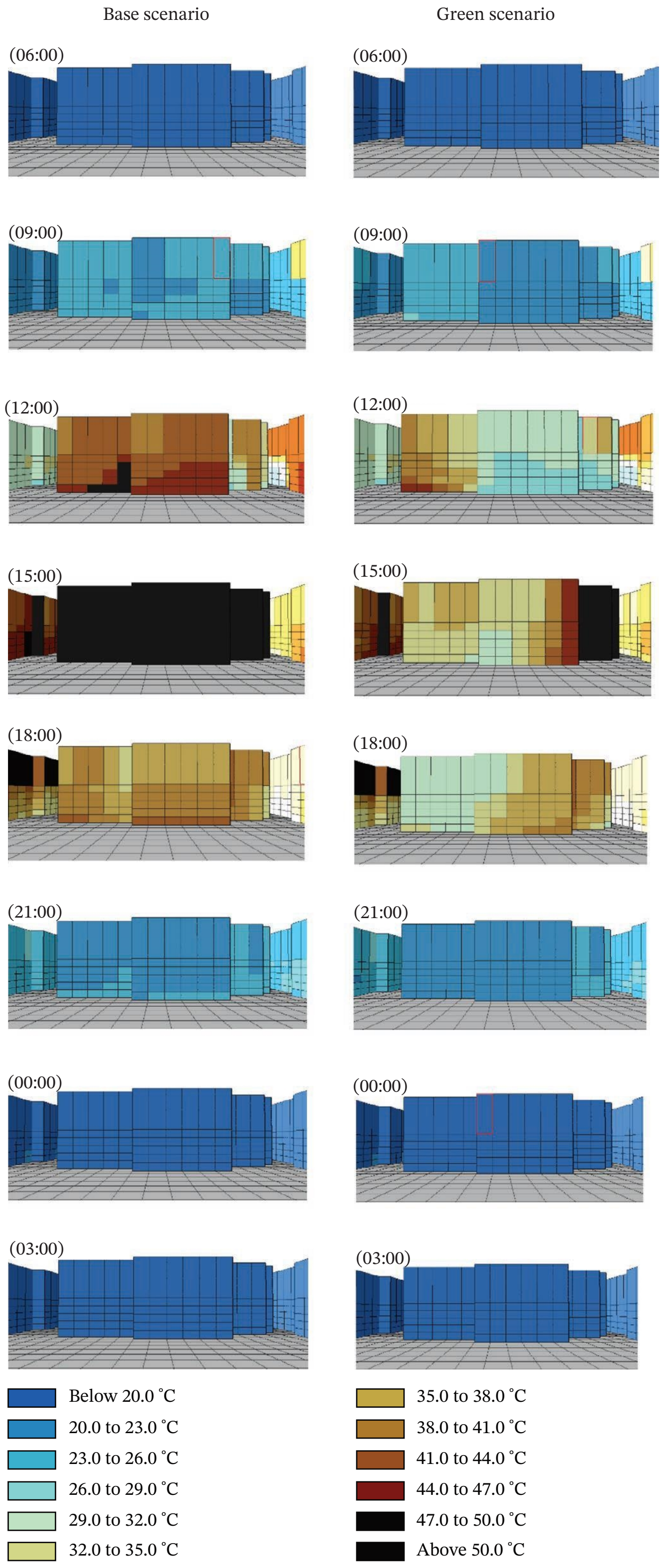

FIGURE 11 | Thermal imagery of façade surface temperatures (T_{ow}) under Base and Green scenarios at 3-h intervals.

It should be noted that the T_{in} reported here is derived from ENVI-met's simplified indoor module and is therefore intended to indicate relative differences between scenarios rather than absolute indoor thermal conditions.

3.9 | Summary of Results

Table 6 summarises the maximum hourly reductions in key outdoor microclimatic parameters between the Base and

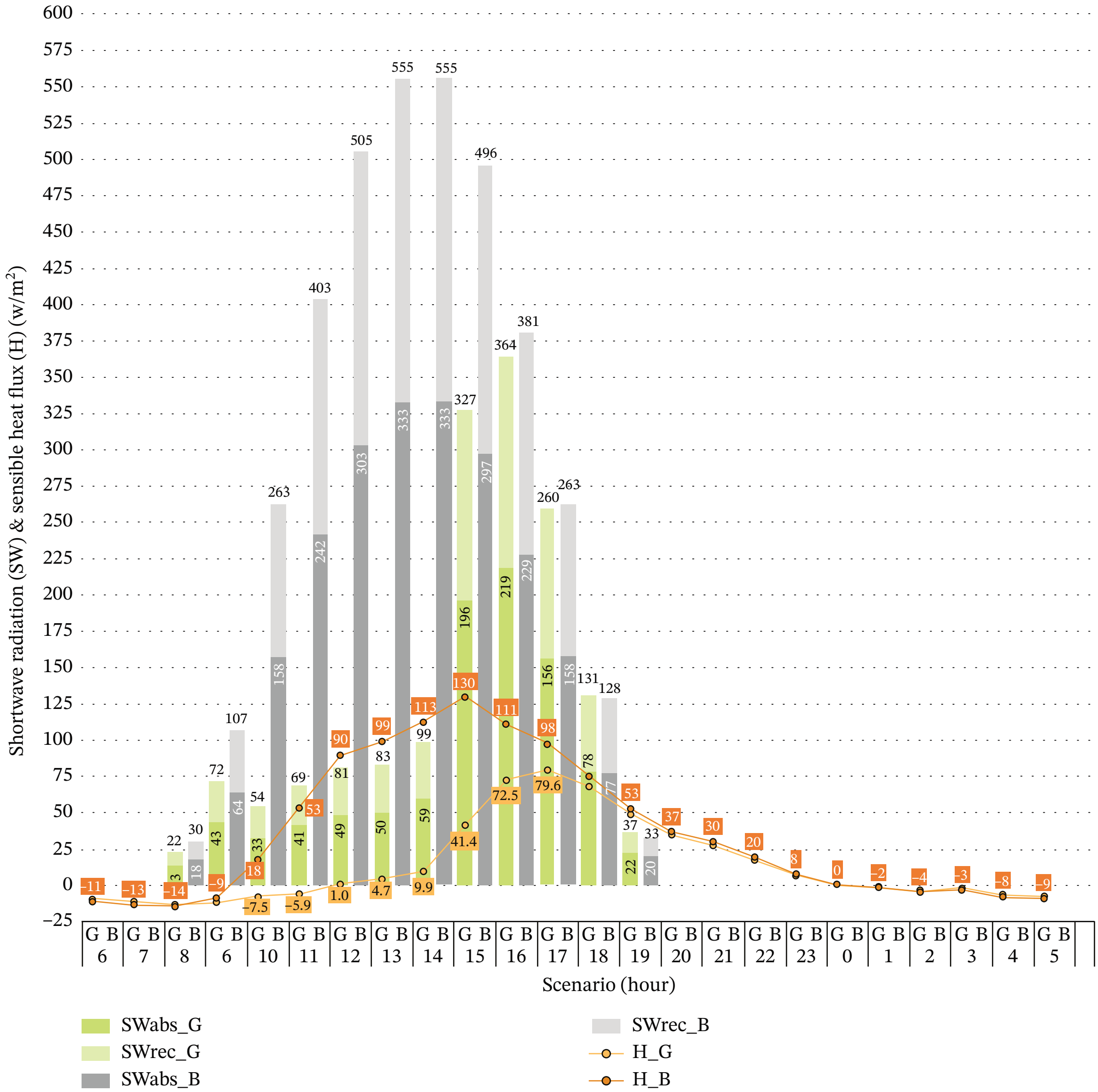

FIGURE 12 | Stacked bars show shortwave radiation received and absorbed by the façade (Base vs. Green), whereas lines show sensible heat flux (H) over 24 h (Base vs. Green).

Green scenarios at various locations. The comparative analysis indicates that strategically positioned vegetation—aligned with solar orientation and façade geometry—significantly strengthens the thermal buffer between greenery and the building envelope. PET and MRT exhibited consistent diurnal patterns across locations, but with notable spatial differences. Under the Base scenario, near-building locations exhibited higher PET and MRT values compared with the pedestrian pathway, confirming that façades intensify thermal stress through reflected radiation and reduced ventilation. Conversely, under the Green scenario, these near-building conditions were markedly improved, with PET and MRT levels approaching those observed near the pathway. The magnitude of the reported PET and MRT reductions reflects peak, localised conditions rather than domain-wide averages. These maximum reductions occurred during early afternoon hours (around 14:00–15:00) at the façade-adjacent location (Location A), where direct solar exposure in the Base scenario was replaced by near-complete canopy shading in the Green scenario. MRT is highly sensitive to shortwave radiation and surface temperatures, and therefore responds nonlinearly to shading interventions. The large reductions observed here are primarily driven by radiative attenuation and reduced view factors to hot surfaces, rather than by changes in T_a, which remained comparatively modest. These results confirm that well-designed front-yard greenery can effectively mitigate façade-induced heat stress, enhance outdoor thermal comfort and reduce thermal load on adjacent building surfaces. Given the limited height and shading extent of hedges compared with trees, their influence on the simulated microclimatic parameters was secondary and primarily confined to near-surface humidity and airflow modulation.

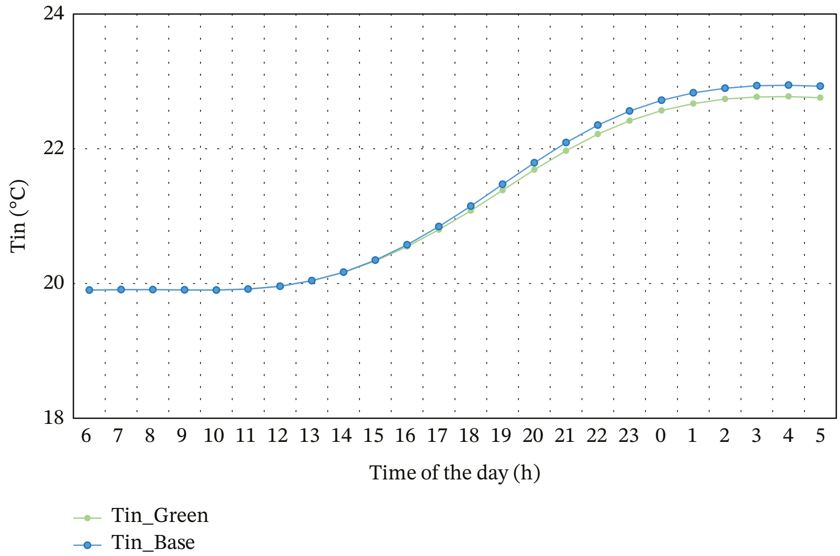

(a)

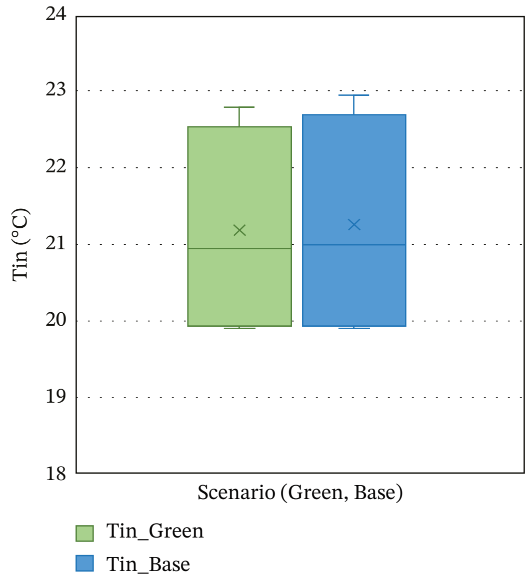

(b)

FIGURE 13 | Comparison of indicative T_{in} for Base and Green scenarios based on (a) diurnal trend over the 24-h simulation period; (b) distribution of hourly values, showing minimum, maximum, median (line) and mean (×).

4 | Discussion

The discussion is structured to first interpret direct microclimatic outcomes, then contextualise inferred indoor implications and finally situate the findings within existing literature and acknowledged methodological limitations.

This study examined how buffer zone vegetation can modify near-building microclimates within a low-greenery residential setting. Indoor relevance is further quantified using ENVI-met's indicative indoor module as a comparative proxy, which represents the building interior as a single thermal zone coupled to the outdoor microclimate. These results are used to assess relative differences between scenarios rather than as full indoor thermal comfort or IAQ assessments. The present discussion is therefore grounded in a descriptive, scenario-based interpretation of deterministic simulation outputs rather than statistical inference. Result stability is assessed through consistent diurnal trends and spatial contrasts across multiple receptor locations rather than through probabilistic variability metrics. Inferred indoor implications are derived from established physical linkages between near-façade outdoor microclimate, heat transfer across the building envelope and ventilation-driven air exchange, with T_{in} outputs serving as a quantitative indicator of relative indoor response. Accordingly, the discussion adopts a mechanism-based interpretative approach rather than direct quantification of indoor responses. The findings demonstrate substantial reductions in PET, MRT, façade surface temperature and H under the Green scenario compared with the Base case, particularly near the building façade. These align with known mechanisms linking outdoor environmental modifications to indoor responses, including infiltration-driven

TABLE 5 | Indicative indoor thermal proxy metrics.

Indicator	Period	Difference (green-base)	Notes
Mean T_{in}	14:00–22:00	−0.1°C	Representative daytime–evening cooling
Max T_{in}	22:00–02:00	−0.2°C	Instantaneous peak reduction
Cumulative indoor cooling	14:00–22:00	0.7°C.h	Daytime–evening cumulative effect
Cumulative indoor cooling	24 h	1.7°C.h	Persistence across full simulation period

TABLE 6 | Maximum hourly changes in values of key output parameters between Base and Green scenarios.

Parameter	Location	Change*	Time	Dominant mechanism
PET	A	↓ 17.1°C	15:00	Shading + evapotranspiration
	B	↓ 12.4°C	16:00	Shading + evapotranspiration
	C	↓ 0.7°C	17:00	
MRT	A	↓ 32.7°C	15:00	Radiative interception
	B	↓ 26.0°C	16:00	Radiative interception
	C	↓ 1.1°C	17:00–18:00	
T_a	A	↓ 0.9°C	15:00	
	B	↓ 0.7°C	16:00	
	C	↓ 0.3°C	16:00–17:00	
RH	A	↑ 2.5%	16:00	
	B	↑ 1.9%	16:00–17:00	
	C	↑ 1.9%	17:00	
Wind speed	A, B, C	≤0.5 m/s		
T_{ow}		↓ 22.0°C	14:00	Reduced solar load
T_{iw}		↓ 0.8°C	22:00–02:00	
SW radiation (rec.)		↓ 472.0 W/m^2	13:00	Canopy shading
SW radiation (abs.)		↓ 283.2 W/m^2	13:00	Canopy shading
Sensible heat flux		↓ 103.1 W/m^2	14:00	Reduced surface heating
T_{in} (indicative)	Indoor	↓ 0.2°C	22:00–02:00	Envelope cooling via reduced façade heat transfer

[a]Changes are calculated as Base – Green. Arrows show the direction of change compared with the Base scenario (↑ increase, ↓ reduction).

pollutant transport, conductive and radiative heat gains and ventilation-mediated thermal exchange.

4.1 | Linking Outdoor Modifications to IAQ and Thermal Comfort

Outdoor air quality, humidity, wind patterns and façade boundary conditions are key determinants of IAQ and thermal comfort. From an indoor environmental science perspective, near-façade microclimatic conditions represent a critical interface through which outdoor environmental forcing is transmitted indoors, particularly in naturally ventilated residential buildings. Prior studies highlight that window operation, occupancy and ventilation strategies strongly influence pollutant penetration and removal [48], whereas shading, vegetation and façade design reduce solar gains and moderate stabilise near-wall temperature (Table 2). The reductions in PET, MRT, façade surface temperature and H are directly derived from the ENVI-met simulations and form the evidentiary basis for the subsequent mechanism-based discussion. Although the present modelling framework does not explicitly decompose the individual contributions of shading, evapotranspiration and airflow modification, their relative influence is inferred based on the magnitude and timing of changes in radiation, surface temperature and thermal comfort indices, consistent with established urban microclimate theory. While hedges were included in the Green scenario, their lower height and limited canopy volume constrained their contribution mainly to near-ground microclimatic modulation, such as marginal increases in RH and subtle airflow deflection. The marked reductions in PET and MRT at Location A (adjacent to the façade) therefore indicate tangible improvements in the immediate outdoor environment governing the air and heat exchange at the building envelope.

Indicative T_{in} outputs show small but consistent reductions of 0.1°C–0.2°C under the Green scenario, with the peak reduction (~0.2°C) occurring during evening and early night hours (22:00–02:00). The cumulative 24-h difference in T_{in} amounts to approximately 1.7°C.h, demonstrating that façade-scale microclimatic improvements translate into a modest but persistent indoor thermal effect. These reductions coincide temporally with the largest façade surface temperature and H reductions, confirming that outdoor radiative and convective mitigation directly influence indoor thermal conditions.

Indoor pollutant concentrations typically reach 44%–60% of outdoor levels under natural ventilation [25]. Among external factors, outdoor humidity, window opening and occupancy are the primary determinants of the infiltration factor (F_{inf}) [48], which represents the equilibrium fraction of outdoor particles that penetrate and remain airborne indoors. Reported F_{inf} values range from 0.3–0.82 for $PM_{2.5}$ and 0.17–0.52 for PM_{10}, with higher values for finer particles due to reduced deposition rates [68]. In some cases, F_{inf} for $PM_{2.5}$ extends from 0.51 to 1.16, depending on season, floor level and building characteristics [49]. Therefore, vegetative buffers may improve IAQ in principle by reducing near façade pollutant exposure and modifying infiltration-relevant boundary conditions, as reported in prior studies.

The observed reduction in exterior wall temperature (mean 4.4°C, peak 22°C) and H further suggest diminished conductive and convective heat transfer through the building envelope. Previous research reports that such reductions can lower T_{in} by 1°C–3.4°C and reduce pollutant infiltration rates, particularly for $PM_{2.5}$ and NO_2, when combined with natural ventilation [23, 51]. Although a detailed indoor thermal and IAQ model was not implemented, the ENVI-met single-zone T_{in} proxy indicates meaningful indoor benefits in both thermal comfort and IAQ.

Overall, the results confirm that radiative and surface-energy exchanges are the dominant mechanisms through which private greenery improves near-building microclimates. Although T_a and humidity exhibited modest changes, substantial reductions in MRT and PET highlight the critical role of radiation interception and localised shading in regulating thermal exposure. Table 7 compares the findings of this study with results from previous research. Comparisons with studies are intended to contextualise the magnitude of observed microclimatic effects rather than imply direct equivalence, given differences in modelling scope and evaluation of metrics.

The comparative analysis in Table 7 shows that the present study reductions in PET (17.1°C) and MRT (32.7°C) fall within, and in some cases exceed, the upper range reported in previous research. This confirms that even small front-yard vegetation buffers can deliver microclimatic benefits comparable with those achieved by larger urban greening interventions. The 22.0°C reduction in façade surface temperature is also consistent with other shading-based studies [51, 53], demonstrating that vegetation can substantially limit solar heat gains at the building envelope. Although indoor energy performance was not directly simulated, the magnitude of façade temperature reduction and H attenuation observed in this study is comparable with outdoor microclimatic changes reported in previous research that achieved peak cooling load reductions of approximately 10%–20%. These values are cited here to contextualise the potential scale of impact rather than to imply a direct quantitative outcome of the present simulations.

4.2 | Implications for Energy and Building Performance

Reduced façade radiation loads and exterior surface temperatures have direct implications for cooling energy demand. Previous studies have reported 5%–21.7% decreases in cooling loads when façade shading or vegetation were applied [23, 52, 53]. In the present study, the combined reduction in shortwave radiation (82% reduction during peak hours) and H (~39% at peak) indicates a substantial decline in external thermal loads acting on the building envelope. The observed reductions in T_{in}, though modest, reinforce that these façade-scale changes translate into small but persistent indoor cooling. The cumulative 24-h cooling effect (~1.7°C.h) highlights the potential energy benefit under natural or mixed-mode ventilation.

From an applied perspective, these results emphasise the practicality of private front-yard greenery as a small-scale but effective thermal-mitigation measure in compact residential environments. Integrating well-designed vegetation buffers near façades can moderate the immediate microclimate, limit heat and pollutants exposure and enhance occupant comfort without structural modification. Embedding such evidence-based greening measures into local building codes, sustainability assessment schemes and urban-resilience guidelines would help connect outdoor microclimate regulation with indoor environmental quality, ultimately supporting lower household energy consumption and improved health outcomes.

4.3 | Limitations

There are several limitations, as follows:

1. Proxy-based indoor assessment

T_{in} outputs are derived from ENVI-met's simplified single-zone module and should be interpreted as comparative indicators rather than absolute indoor thermal conditions. Full indoor comfort indices and IAQ metrics were not simulated.

TABLE 7 | Comparison of results to other studies.

Parameter	Study	Variation	Description
PET	Current	↓ 17.1°C	Peak hour (15:00), Location A
	[52]	↓ 21°C	Depending on the local climate zone (LCZ) and tree species
MRT	Current	↓ 32.7°C	Peak hour (15:00), Location A
	[22]	↓ ~6°C–8°C	
T_{ow}	Current	↓ 22.0°C	Peak hour (14:00)
	[53]	↓ 20°C	East-west wall under full shading
	[51]	↓ ~6°C	Buildings shaded ≥ 6 h
T_{in}	Current	↓ 0.1°C–0.2°C	Indicative T_{in}
	[23, 51]	↓ 1°C–3.4°C	
PMV	[22]	↑ 2.6–2.7	Indoor thermal comfort parameter
Building cooling load	[53]	↓ 10%–15.2%	
	[69]	↓ 4.5%–10.2%	
	[66]	↓ 5%–21.7%	Peak cooling load, depending on tree orientation
	[23]	↓ 15%–20%	Peak cooling load, at midday across four cities
Energy saving rate	[52]	↑ 0.9%–8%	Depending on LCZ and tree species

2. Temporal and climatic scope

The analysis was limited to a single clear-sky summer day selected to represent peak thermal stress conditions, and therefore does not capture seasonal variability, overcast or rainy conditions or extreme heatwave events. As such, the results reflect short-term summer performance rather than year-round or long-term microclimatic behaviour. In addition, the study does not account for climate change–driven increases in heatwave frequency or intensity, which may amplify both the benefits and limitations of vegetation-based mitigation strategies.

3. Model uncertainty and parameter sensitivity

Sensitivity and uncertainty analyses were not conducted for vegetation parameters, material properties or boundary conditions. Although prior ENVI-met validation studies were referenced, the present work prioritised relative comparisons between scenarios under identical conditions.

4. Simplified vegetation representation

Vegetation was modelled as static and idealised, without accounting for growth cycles, physiological responses, irrigation or maintenance effects that influence shading and evapotranspiration performance.

5. Exclusion of behavioural and economic factors

Occupant behaviour, energy-use patterns and economic feasibility were not considered, although these factors influence the real-world effectiveness and adoption of residential greening strategies.

4.4 | Transferability and Future Directions

Although this case study is site-specific, the buffer-zone vegetation framework represents a modular and transferable approach for improving near-building microclimates in low-rise residential urban forms. The findings are most directly applicable to midlatitude temperate climates characterised by high summer solar exposure, moderate wind speeds and detached or semidetached dwellings with shallow front setbacks (~4–10 m), such as those typical of Australian, Southern European and parts of North American suburbs.

With appropriate adjustments for local meteorology, solar geometry and vegetation characteristics, the methodology can also inform design in hot–dry climates, where shading-driven reductions in radiative load dominate thermal performance, and in subtropical cities, where shading remains critical but evapotranspirative cooling may be moderated by higher background humidity. In all cases, the dominant mechanisms—radiative interception, façade shading and near-surface airflow modification—remain physically consistent, supporting cross-climatic applicability within comparable urban morphologies.

The framework can be extended to different yard orientations (east-, west- and south-facing) and other private open spaces such as backyards, courtyards and semienclosed shared spaces, enabling assessment of cumulative cooling and air-quality benefits at the neighbourhood scale. Future studies should also integrate ENVI-met simulations with dynamic building energy and IAQ models (e.g., EnergyPlus and CONTAM) to explicitly quantify indoor thermal and air quality responses. Application beyond these contexts, including high-rise districts, deep street canyons or areas with extensive existing tree canopy, would require reconfiguration of vegetation placement and additional modelling to account for altered radiative and aerodynamic regimes.

Future research should extend the present framework to long-term simulations across multiple seasons, weather conditions and extreme heat events to evaluate the persistence and variability of vegetation-induced benefits. In particular, year-round analysis is needed to assess the seasonal trade-offs associated with deciduous tree species, including enhanced winter solar access, daylight availability and potential impacts on space-heating demand. Such seasonal and life-cycle evaluation is essential for understanding the full climatic and energy implications of front-yard greening under both current and future climate scenarios. Incorporating species-specific vegetation parameters, sensitivity analyses and plant physiological dynamics would further enhance robustness. Finally, integrating behavioural, economic and maintenance considerations would support the translation of microclimate modelling outcomes into practical, evidence-based residential design and planning guidelines.

5 | Conclusion

This study investigated how vegetation in private front-yard buffer zones modifies near-façade microclimates in low-greenery residential contexts, focusing on outdoor environmental drivers relevant to indoor conditions. Using ENVI-met simulations for a generic low-rise dwelling under two contrasting scenarios, a fully paved yard and a vegetated configuration incorporating trees and hedges, the analysis isolated vegetation-induced microclimatic effects at the building envelope. The results demonstrate that front-yard vegetation substantially reduces near-façade thermal stress, with peak-hour reductions of approximately 17°C in PET and 33°C in MRT, alongside a 22°C decrease in façade surface temperature and a reduction in H of about 103 W/m^2. Indicative T_{in} proxies showed consistent but modest reductions of 0.1°C–0.2°C, with a cumulative 24-h effect of 1.7°C, aligned with façade-scale cooling. In contrast, changes in T_a and humidity were comparatively small, indicating that radiative interception and surface-energy regulation dominate the cooling mechanism. These findings establish the façade-scale microclimate as a critical physical interface through which outdoor vegetation conditions heat and airflow at the building envelope, providing quantitative boundary-condition evidence relevant to indoor thermal comfort, air quality and cooling demand. These results demonstrate that front-yard vegetated buffers serve as an effective building-scale microclimatic regulator, modifying façade-level radiative and thermal drivers that influence heat transfer and ventilation-mediated indoor conditions. Future research should extend this framework by coupling outdoor microclimate models with dynamic indoor energy and IAQ simulations, and by testing multiple seasons, climatic contexts and vegetation configurations to support more generalisable design guidance.

Nomenclature

BoM	Bureau of Meteorology (Australia)
CFD	computational fluid dynamics
EPW	EnergyPlus Weather file
F_i	landscaping isolation index (layout index used to characterise vegetation configuration)
F_{inf}	infiltration factor (fraction of outdoor particles penetrating indoors)
H	sensible heat flux
IAQ	indoor air quality
LAI	leaf area index
LAD	leaf area density
LCZ	local climate zone
MRT	mean radiant temperature
NO_2	nitrogen dioxide
O_3	ozone
PET	physiological equivalent temperature
$PM_{2.5}$	particulate matter with aerodynamic diameter $\leq 2.5\,\mu m$
PM_{10}	particulate matter with aerodynamic diameter $\leq 10\,\mu m$
RH	relative humidity
T_a	air temperature
T_{in}	indoor temperature
T_{iw}	inside wall temperature
T_{ow}	outside wall temperature

Acknowledgments

During the preparation of this work, the authors used an OpenAI tool to enhance language and readability. After using the tool, the authors reviewed and edited the content as needed. The authors highlight that AI's role was to assist in refining the text and language, and not to replace any critical tasks of the authors.

Funding

This study was supported by an Australian Government Research Training Program (RTP) Scholarship 10.82133/C42F-K220 and the Commonwealth Scientific and Industrial Research Organisation (CSIRO), PhD Top-Up Fund (Position Number: 50100673).

Disclosure

The authors take full responsibility for the final content of the publication.

Conflicts of Interest

The authors declare no conflicts of interest.

Data Availability Statement

The ENVI-met simulation input files, model configuration parameters and postprocessing scripts generated during this study are available from the corresponding author upon reasonable request. Due to large file sizes and dependence on proprietary software environments, these materials are not publicly archived at this stage. Requests for access will be considered to support transparency and reproducibility.

References

1. Q. Wu, Y. Huang, P. Irga, et al., "Synergistic Control of Urban Heat Island and Urban Pollution Island Effects Using Green Infrastructure," *Journal of Environmental Management* 370 (2024): 122985, https://doi.org/10.1016/j.jenvman.2024.122985.

2. W. Che, and W. Zhuang, "Integrated Vegetation Effects on Thermal Environment and Air Quality in Urban Street Canyons," *Urban Climate* 63 (2025): 102593, https://doi.org/10.1016/j.uclim.2025.102593.

3. U. K. Priya, and R. Senthil, "Enhancing Sustainable Urban Planning to Mitigate Urban Heat Island Effects Through Residential Greening," *Sustainable Cities and Society* 129 (2025): 106512, https://doi.org/10.1016/j.scs.2025.106512.

4. X. Yang, L. Yao, M. Li, et al., "How Heat Waves and Urban Microclimates Affect Building Cooling Energy Demand? Insights From Fifteen Eastern Chinese Cities," *Applied Energy* 384 (2025): 125424, https://doi.org/10.1016/j.apenergy.2025.125424.

5. J. Kim, S. Yeom, and T. Hong, "Analyzing the Cooling Effect, Thermal Comfort, and Energy Consumption of Integrated Arrangement of High-Rise Buildings and Green Spaces on Urban Heat Island," *Sustainable Cities and Society* 119 (2025): 106105, https://doi.org/10.1016/j.scs.2024.106105.

6. Z. Liu, K. Y. Cheng, T. Sinsel, et al., "Modeling Microclimatic Effects of Trees and Green Roofs/Façades in ENVI-met: Sensitivity Tests and Proposed Model Library," *Building and Environment* 244 (2023): 110759, https://doi.org/10.1016/j.buildenv.2023.110759.

7. M. Hosseini, K. Javanroodi, and V. M. Nik, "High-Resolution Impact Assessment of Climate Change on Building Energy Performance Considering Extreme Weather Events and Microclimate–Investigating Variations in Indoor Thermal Comfort and Degree-Days," *Sustainable Cities and Society* 78 (2022): 103634, https://doi.org/10.1016/j.scs.2021.103634.

8. I. L. Niza, A. M. Bueno, M. Gameiro da Silva, and E. E. Broday, "Air Quality and Ventilation: Exploring Solutions for Healthy and Sustainable Urban Environments in Times of Climate change," *Results in Engineering* 24 (2024): 103157, https://doi.org/10.1016/j.rineng.2024.103157.

9. G. P. Kenny, E. J. Tetzlaff, W. S. Journeay, S. B. Henderson, and F. K. O'Connor, "Indoor Overheating: A Review of Vulnerabilities, Causes, and Strategies to Prevent Adverse Human Health Outcomes During Extreme Heat Events," *Temperature* 11, no. 3 (2024): 203–246, https://doi.org/10.1080/23328940.2024.2361223.

10. J. Yang, J. Duan, X. Niu, et al., "A Comprehensive Review on Indoor Air Pollutants and Their Health Impacts: Priority Pollutants and Suggested Mitigations," *Air Quality, Atmosphere & Health* 18, no. 7 (2025): 2151–2184, https://doi.org/10.1007/s11869-025-01750-3.

11. Y. Zhao, R. Li, J. Niu, X. Shi, and N. Gao, "Numerical Simulation of Diurnal and Nocturnal Impact of Vegetated Facades on Microclimate," *Building and Environment* 279 (2025): 113063, https://doi.org/10.1016/j.buildenv.2025.113063.

12. J. Ge, Y. Wang, D. Zhou, Z. Gu, and X. Meng, "Effects of Urban Vegetation on Microclimate and Building Energy Demand in Winter: An Evaluation Using Coupled Simulations," *Sustainable Cities and Society* 102 (2024): 105199, https://doi.org/10.1016/j.scs.2024.105199.

13. A. Baghaei Daemei, and A. Jamali, "Experimental and Simulation Study on Thermal Effects and Energy Efficiency of a Green Wall in the Humid Condition of Rasht," *Journal of Energy Management and Technology* 6, no. 1 (2022): 15–21, https://doi.org/10.22109/jemt.2021.250352.1258.

14. N. Halder, M. Kumar, A. Deepak, et al., "The Role of Urban Greenery in Enhancing Thermal Comfort: Systematic Review Insights," *Sustainability* 17, no. 6 (2025): 2545, https://doi.org/10.3390/su17062545.

15. Y. Zhao, R. Li, J. Niu, X. Shi, and N. Gao, "Impact of Vegetated Facades on Microclimate and Outdoor Thermal Comfort Across Different Building Morphologies," *Building and Environment* 285 (2025): 113614, https://doi.org/10.1016/j.buildenv.2025.113614.

16. X. Yue, W. Liu, X. Wang, et al., "Constructing an Urban Heat Network to Mitigate the Urban Heat Island Effect From a Connectivity Perspective," *Sustainable Cities and Society* 114 (2024): 105774, https://doi.org/10.1016/j.scs.2024.105774.

17. P. Kumar, S. E. Debele, S. Khalili, et al., "Urban Heat Mitigation by Green and Blue Infrastructure: Drivers, Effectiveness, and Future needs," *Innovation* 5, no. 2 (2024): 100588, https://doi.org/10.1016/j.xinn.2024.100588.

18. S. Yang, L.(L.) Wang, T. Stathopoulos, and A. M. Marey, "Urban Microclimate and Its Impact on Built Environment-A Review," *Building and Environment* 238 (2023): 110334, https://doi.org/10.1016/j.buildenv.2023.110334.

19. C. Silveira, A. T. C. Dias, F. G. Amaral, G. de Gois, and N. Pistón, "The Importance of Private Gardens and Their Spatial Composition and Configuration to Urban Heat Island Mitigation," *Sustainable Cities and Society* 112 (2024): 105589, https://doi.org/10.1016/j.scs.2024.105589.

20. U. K. Priya, and R. Senthil, "Framework for Enhancing Urban Living Through Sustainable Plant Selection in Residential Green Spaces," *Urban Science* 8, no. 4 (2024): 235, https://doi.org/10.3390/urbansci8040235.

21. I. Vigevani, D. Corsini, S. Comin, A. Fini, and F. Ferrini, "Methods to Quantify Particle Air Pollution Removal by Urban Vegetation: A Review," *Atmospheric Environment: X* 21 (2024): 100233, https://doi.org/10.1016/j.aeaoa.2023.100233.

22. L. Rui, R. Buccolieri, Z. Gao, W. Ding, and J. Shen, "The Impact of Green Space Layouts on Microclimate and Air Quality in Residential Districts of Nanjing, China," *Forests* 9, no. 4 (2018): 224, https://doi.org/10.3390/f9040224.

23. X. Xiao, J. Yuan, Z. Jiao, et al., "Shading Effects On Building Energy Performance: A Multi-City Analysis," *Results in Engineering* 27 (2025): 106870, https://doi.org/10.1016/j.rineng.2025.106870.

24. L. Feng, L. Shuai, Y. Zhou, X. Zhang, and J. Sun, "Improving the Green Space Arrangement in Residential Areas From the Perspective of Tree Leaf Temperature Utilizing Scenario Simulation in ENVI-met," *Science of The Total Environment* 918 (2024): 170650, https://doi.org/10.1016/j.scitotenv.2024.170650.

25. B. Hong, H. Qin, R. Jiang, M. Xu, and J. Niu, "How Outdoor Trees Affect Indoor Particulate Matter Dispersion: CFD Simulations in a Naturally Ventilated Auditorium," *International Journal of Environmental Research and Public Health* 15, no. 12 (2018): 2862, https://doi.org/10.3390/ijerph15122862.

26. J. Linden, M. Gustafsson, J. Uddling, Å. Watne, and H. Pleijel, "Air Pollution Removal Through Deposition on Urban Vegetation: The Importance of Vegetation Characteristics," *Urban Forestry & Urban Greening* 81 (2023): 127843, https://doi.org/10.1016/j.ufug.2023.127843.

27. M. Vashist, T. V. Kumar, and S. K. Singh, "A Comprehensive Review of Urban Vegetation as a Nature-Based Solution for Sustainable Management of Particulate Matter in Ambient Air," *Environmental Science and Pollution Research* 31, no. 18 (2024): 26480–26496, https://doi.org/10.1007/s11356-024-33089-0.

28. G. Miller, and L. Morawska, "State of Indoor Air in Australia 2025: The First Comprehensive Assessment of Australia's Indoor Air Quality. 2025, THRIVE Collaborative for Healthy Buildings and Air Quality: Brisbane, Australia," https://thriveiaq.com/wp-content/uploads/2025/10/20250909-State-of-Indoor-Air-in-Australia-final.pdf?utm_source=chatgpt.com.

29. R. Khalvandi, and M. Karimimoshaver, "Urban Street Canyons and Heat Islands: A Systematic Review on Morphological Solutions," *Results in Engineering* 27 (2025): 106542, https://doi.org/10.1016/j.rineng.2025.106542.

30. J. Yang, Z. Wu, M. Menenti, et al., "Impacts of Urban Morphology on Sensible Heat Flux and Net Radiation Exchange," *Urban Climate* 50 (2023): 101588, https://doi.org/10.1016/j.uclim.2023.101588.

31. R. Widiastuti, J. Zaini, W. Caesarendra, G. Kokogiannakis, and S. N. N. Binti Suhailian, "Thermal Insulation Effect of Green Façades Based on Calculation of Heat Transfer and Long Wave Infrared Radiative Exchange," *Measurement* 188 (2022): 110555, https://doi.org/10.1016/j.measurement.2021.110555.

32. I. Blanco, and F. Convertino, "Thermal Performance of Green Façades: Research Trends Analysis Using a Science Mapping Approach," *Sustainability* 15, no. 13 (2023): 9981, https://doi.org/10.3390/su15139981.

33. M. Rouhollahi, M. Behrend, and J. Boland, "Optimising Tree Arrangement Policy in Australian Small-Scale Residential Settings," *Sustainable Cities and Society* 102 (2024): 105232, https://doi.org/10.1016/j.scs.2024.105232.

34. L. Morawska, J. Allen, W. Bahnfleth, et al., "Mandating Indoor Air Quality for Public Buildings," *Science* 383, no. 6690 (2024): 1418–1420, https://doi.org/10.1126/science.adl0677.

35. EPA-Victoria, "Air Pollution Sources in Inner West Melbourne," (Environment Protection Authority, 2025)https://www.epa.vic.gov.au/air-pollution-sources-inner-west-melbourne.

36. Air_Quality_Community_Reference_Group, "Air Pollution in Melbourne's Inner West," (2020), https://www.environment.vic.gov.au/__data/assets/pdf_file/0030/486507/IWAQCRGSummaryReportFINAL.pdf?.

37. R. Fedele, P. Davy, M. Keywood, et al., "Air Pollution Sources in Inner West Melbourne," (2024)https://www.epa.vic.gov.au/-/media/epa/files/publications/2060---air-pollution-sources-in-inner-west-melbourne.pdf?la=en%26hash=FB6DF5E7E2ED019F89EA3CDD40498066.

38. The-State-of-Victoria-Department-of-Environment-Land-Water-and-Planning, "Clean Air for All Victorians," (2022), https://www.environment.vic.gov.au/__data/assets/pdf_file/0032/603977/Victorias-air-quality-strategy.pdf.

39. State-of-Victoria-Department-of-Transport-and-Planning, "Victoria in Future 2023 - Population and Household Projections to 2051," (2023), https://www.planning.vic.gov.au/__data/assets/pdf_file/0022/703453/DTP0552-Victori-in-Future-2023-report.PDF.

40. "The Bureau of Meteorology: Climate Data Online," (2025)https://www.bom.gov.au/.

41. Department of Transport and Planning, "Understanding the Residential Development Provisions (ResCode)," (2024), https://www.planning.vic.gov.au/guides-and-resources/guides/planning-practice-notes/understanding-the-residential-development-provisions?utm.

42. Victoria State Government, "More Trees for a Cooler Greener West," (2023), https://www.environment.vic.gov.au/more-trees-for-a-cooler-greener-west/program/about-the-program.

43. Greening the West, "A Regional Approach To Delivering Community Health And Well Being: Strategic Plan 2020-2050," (2020), https://greeningthewest.org.au/wp-content/uploads/2020/12/GTW-StrategicPlan2020-2050-v23.pdf.

44. J. Hurley, "Urban Policy and Planning-A Countermeasure to Urban Heat (IC2UHI)," (2023), https://www.ic2uhi2023.com/.

45. Australian Government Bureau of Meteorology Melbourne, "Climate Statistics for Australian Locations," (2023), https://www.bom.gov.au/climate/averages/tables/cw_086282.shtml.

46. M. Milne, R. Liggett, and A. Benson, *Energy Design Tools Group* (University of California Energy Institute, 2022), https://energy-design-tools.aud.ucla.edu/climate-consultant/request-climate-consultant.html.

47. "Google, Maribyrnong, West Melbourne," (2025), https://www.google.com/maps.

48. J. Kim, J. Son, and J. Koo, "Dynamic Estimation of PM2. 5 Penetration and Removal Rates Using Physics-Informed Neural Networks for Indoor Air Quality Management," *Building and Environment* 278 (2025): 113038, https://doi.org/10.1016/j.buildenv.2025.113038.

49. J. Shi, Y. Shen, R. Yuan, et al., "Field Analysis of PM2. 5 Infiltration Factor and Determinants of Indoor Concentrations in Residential Buildings Within a Mega-City in Southern China," *Atmospheric Environment* 360 (2025): 121433, https://doi.org/10.1016/j.atmosenv.2025.121433.

50. S. Tong, N. H. Wong, E. Tan, and S. K. Jusuf, "Experimental Study on the Impact of Facade Design on Indoor Thermal Environment in Tropical Residential Buildings," *Building and Environment* 166 (2019): 106418, https://doi.org/10.1016/j.buildenv.2019.106418.

51. Y. Park, Q. Zhao, J. M. Guldmann, and E. A. Wentz, "Quantifying the Cumulative Cooling Effects of 3D Building and Tree Shade With High Resolution Thermal Imagery in a Hot Arid Urban Climate," *Landscape and Urban Planning* 240 (2023): 104874, https://doi.org/10.1016/j.landurbplan.2023.104874.

52. Q. Dong, X. Xu, and M. Zhen, "Assessing the Cooling and Buildings' Energy-Saving Potential of Urban Trees in Severe Cold Region of China During Summer," *Building and Environment* 244 (2023): 110818, https://doi.org/10.1016/j.buildenv.2023.110818.

53. C.-M. Hsieh, J. J. Li, L. Zhang, and B. Schwegler, "Effects of Tree Shading and Transpiration on Building Cooling Energy Use," *Energy and Buildings* 159 (2018): 382–397, https://doi.org/10.1016/j.enbuild.2017.10.045.

54. Maribyrnong-City-Council, "Urban Forest Strategy," (2018), https://www.maribyrnong.vic.gov.au/files/assets/public/planning-services-documents/city-design/strategies/urban-forest-strategy-december-2018.pdf.

55. Maribyrnong City Council, "Maribyrnong Street Tree Planting Strategy," (2013), https://www.maribyrnong.vic.gov.au/files/assets/public/planning-services-documents/city-design/strategies/maribyrnong-street-tree-planting-strategy.pdf.

56. D. Kendal, and J. Baumann, "City Of Melbourne's Future Urban Forest: Identifying Vulnerability Vulnerability To Future Temperatures," (2016), https://nespurban.com/wp-content/uploads/2018/11/CAULRR02_CoMFutureUrbanForest_Nov2016.pdf.

57. US Department of Agriculture, "F.S. i-Tree MyTree Tool," (2025)https://mytree.itreetools.org/.

58. M. Wang, Y. Dong, W. Liao, et al., "Impact of Residential Morphology on Outdoor Thermal Comfort and Building Energy Consumption in

Winter and Summer: A Case Study," *Urban Climate* 61 (2025): 102479, https://doi.org/10.1016/j.uclim.2025.102479.

59. W. Ouyang, T. Sinsel, H. Simon, T. E. Morakinyo, H. Liu, and E. Ng, "Evaluating the Thermal-Radiative Performance of ENVI-met Model for Green Infrastructure Typologies: Experience From a Subtropical Climate," *Building and Environment* 207 (2022): 108427, https://doi.org/10.1016/j.buildenv.2021.108427.

60. P. Schöneberger, T. Sinsel, W. Ouyang, Z. Tan, M. Bruse, and H. Simon, "Enhancing Urban Microclimate Simulations: Validating ENVI-met's Accuracy in Modeling Multi-Directional Radiative Fluxes and Mean Radiant Temperature in Subtropical Hong Kong," *Building and Environment* 284 (2025): 113475, https://doi.org/10.1016/j.buildenv.2025.113475.

61. O. Aleksandrowicz, T. Saroglou, and D. Pearlmutter, "Evaluation of Summer Mean Radiant Temperature Simulation in ENVI-met in a Hot Mediterranean Climate," *Building and Environment* 245 (2023): 110881, https://doi.org/10.1016/j.buildenv.2023.110881.

62. E. Jamei, M. Seyedmahmoudian, B. Horan, and A. Stojcevski, "Verification of a Bioclimatic Modeling System in a Growing Suburb in Melbourne," *Science of the Total Environment* 689 (2019): 883–898, https://doi.org/10.1016/j.scitotenv.2019.06.399.

63. Z. Liu, W. Cheng, C. Y. Jim, T. E. Morakinyo, Y. Shi, and E. Ng, "Heat Mitigation Benefits of Urban Green and Blue Infrastructures: A Systematic Review of Modeling Techniques, Validation and Scenario Simulation in ENVI-met V4," *Building and Environment* 200 (2021): 107939, https://doi.org/10.1016/j.buildenv.2021.107939.

64. A. Kianmehr, and T. C. Lim, "Quantifying Interactive Cooling Effects of Morphological Parameters and Vegetation-Related Landscape Features During an Extreme Heat Event," *Climate* 10, no. 4 (2022): 60, https://doi.org/10.3390/cli10040060.

65. X. Zhang, J. W. G. Buddhika, J. Wang, A. U. Weerasuriya, and K. T. Tse, "Numerical Investigation of Effects of Trees on Cross-Ventilation of an Isolated Building," *Journal of Building Engineering* 73 (2023): 106808, https://doi.org/10.1016/j.jobe.2023.106808.

66. K. Zhang, F. Qi, T. Zhang, and L. Zhou, "The Impact of Trees on the Peak Cooling Load of Detached Rural Residences," *Energy and Buildings* 317 (2024): 114311, https://doi.org/10.1016/j.enbuild.2024.114311.

67. M. Taleghani, A. Clark, W. Swan, and A. Mohegh, "Air Pollution in a Microclimate; The Impact of Different Green Barriers on the Dispersion," *Science of the Total Environment* 711 (2020): 134649, https://doi.org/10.1016/j.scitotenv.2019.134649.

68. C. Chen, and B. Zhao, "Review of Relationship Between Indoor and Outdoor Particles: I/O ratio, Infiltration Factor and Penetration Factor," *Atmospheric Environment* 45, no. 2 (2011): 275–288, https://doi.org/10.1016/j.atmosenv.2010.09.048.

69. U. Passe, M. Dorneich, C. Krejci, et al., "An Urban Modelling Framework for Climate Resilience in low-Resource Neighbourhoods," *Buildings and Cities* 1, no. 1 (2020): 453–474, https://doi.org/10.5334/bc.17.

Supporting Information

Additional supporting information can be found online in the Supporting Information section. *(Supporting Information)* Additional supporting information is provided in Appendix Table A1, which summarises broader urban-scale and indirect evidence underpinning the functional pathways linking private outdoor greenery to indoor air quality and thermal comfort. This supporting material complements the main analysis by contextualising the mechanism-based interpretations discussed in Section 4.